BOEING

Electrochemistry of Freshly Generated Titanium Surfaces

Quarterly Progress Report No. 9

SEATTLE, WASHINGTON

CONTRACT NAS 7-489

Stress Corrosion Cracking of Titanium Alloys: Electrochemistry of Freshly Generated Titanium Surfaces

Quarterly Progress Report No. 9

for Period of

July 1, 1968 through September 30, 1968

Prepared by

T.R. Beck

Solid State Physics Laboratory

Boeing Scientific Research Laboratories

Seattle, Washington 98124

TABLE OF CONTENTS

1.0 SUMMARY

The electrochemistry of newly generated surfaces of titanium in acid solutions has been reexamined because calculations with the electrochemical mass-transport-kinetic model for SCC in titanium have indicated that a considerable fraction of the current in a crack may be carried by Ti^{+3} ions. Experiments conducted with rotating disk and ring-disk electrodes in which a titanium disk was scraped with a sapphire cutter in 6 M HCl confirmed that a large fraction of the current to the new surface can be accounted for by formation of Ti^{+3}. The previously obtained kinetic data for titanium in HCl was reinterpreted in the light of the new finding. A patch growth model for the passivating oxide layer shows some promise in fitting the kinetic data and further experiments are underway to test it quantitatively. It is expected that incorporation of the kinetics and transport equations for Ti^{+3} in the MTK model will allow higher potential drops in the crack and thus remove the only serious disagreement so far with the SCC data.

2.0 INTRODUCTION

This report describes part of a study of stress corrosion cracking of titanium alloys initiated in July, 1965 (1) and continued under NASA sponsorship beginning July, 1966 (2). This is the ninth Quarterly Report in the series (3, 4, 5, 6, 7, 8, 9, 10) and covers the period July 1 through September 30, 1968.

Work was continued in two areas in this part quarter: a study of steady-state crack propagation with an aluminum: 2.5% Mg - 6% Zn alloy under potentiostatic conditions in halide solutions, and a reexamination of kinetics of oxidation of freshly generated titanium metal surfaces. The kinetic data and interpretations will be discussed in this report. Work on SCC of aluminum will be summarized in the next Quarterly Report.

3.0 TECHNICAL DISCUSSION

It was decided to reexamine the electrochemistry of freshly generated titanium surfaces because of the apparent requirement for formation of soluble titanium species. Firstly, the mass-transport-kinetic (MTK) model was found to be incapable of producing a potential drop in a crack comparable to experiment assuming all of the current to the walls of the crack forms oxide and hydrogen ion (10). The hydrogen ion formed is in too large a concentration and too conductive to produce a sufficient potential drop. Secondly, the transient potential at interruption of current to a propagating crack (7) suggested the presence of a Ti^{+3}/Ti^{+4} redox couple in the crack.

The objective of reexamination of the electrochemistry was to obtain a quantitative description of the kinetics that is adequate for use in the MTK model. It is desirable to obtain a fundamental understanding of the phenomena, although lacking this, an empirical description might satisfy the MTK model.

Two approaches were used:

1. scraping a titanium disk and measuring the soluble titanium species colorimetrically or by a redox reaction on a gold ring, and
2. an examination of the prior kinetic data for "fine structure" in view of the large fraction of soluble species found in the first approach.

3.1 Theory

Before describing the experimental techniques and results a review of the thermodynamics of the titanium-water system and of some basic equations of electrochemical kinetics is in order.

3.1.1 Thermodynamics

The potential - pH diagram for the titanium-water system is reproduced from Pourbaix (11) in Fig. 1. The diagram gives the fields of stability for the various species under equilibrium conditions.

According to a recent communication by Pourbaix (12) the following hydride equilibria must also be considered (using his numbering system):

25. $2TiH_2 + 3H_2O = Ti_2O_3 + 10H^+ + 10e \qquad E^e = - 0.834 - 0.059\ pH$

26. $TiH_2 = Ti^{++} + 2H^+ + 4e \qquad E^e = - 0.923 - 0.029\ pH + 0.0147\ \log(Ti^{++})$

By these reactions, TiH_2 is the stable phase in contact with water rather than titanium and Fig. 1 should be modified accordingly.

A further change in the diagram is required if the data and analysis of Oliver and Ross (13)* are correct that the standard potential for the $Ti^{+3} - Ti^{+2}$ couple is a -2.3v rather than -0.37v as used by Latimer (14) and by Pourbaix (11). Such a negative potential for this couple would require that titanium be oxidized directly to Ti^{+3}:

---

*My thanks to Dr. Ken Nobe of UCLA for pointing out this paper.

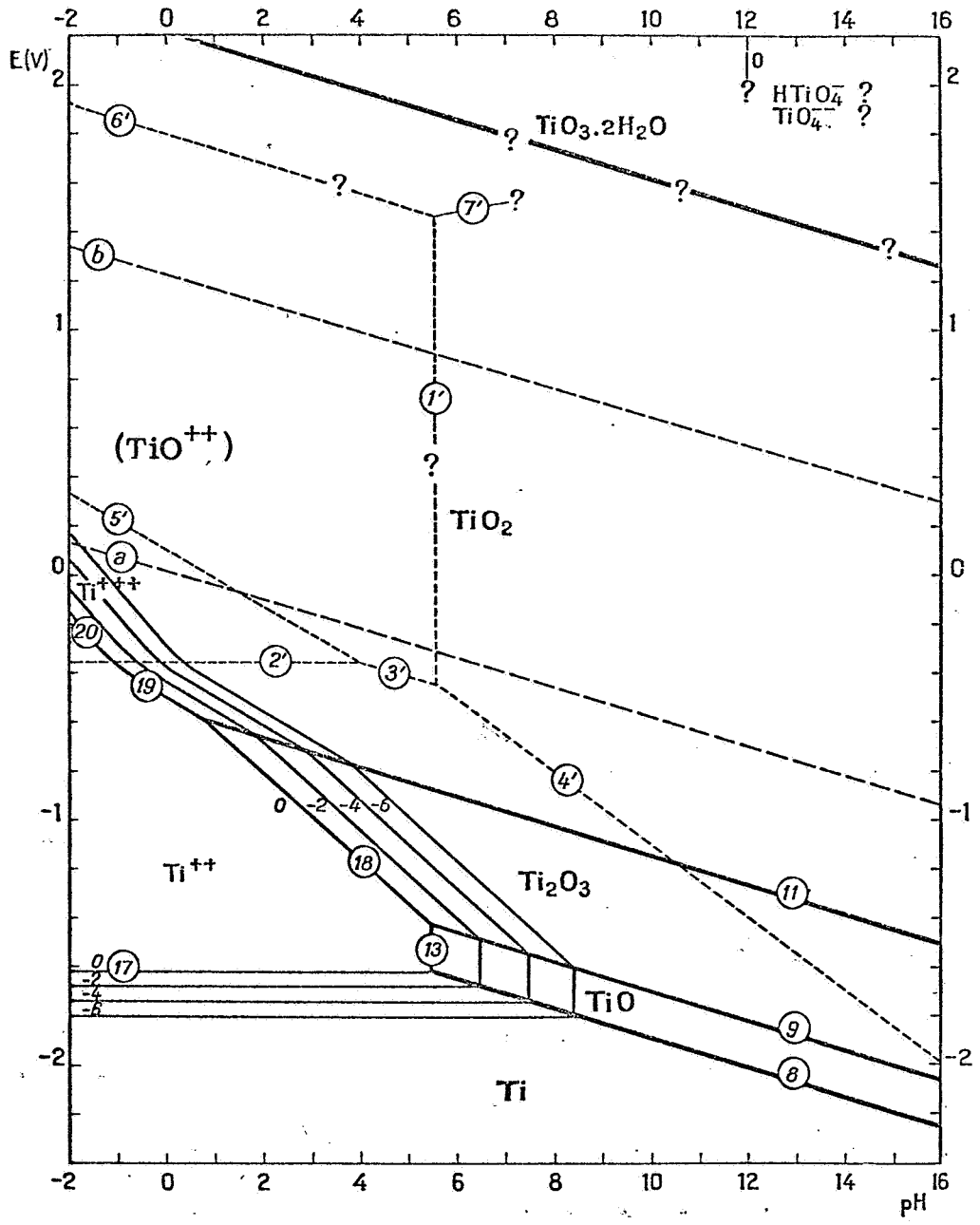

Fig. 1 Potential-pH equilibrium diagram for the system titanium-water, at 25°C. [Figure established by considering, as derivatives of tri- and tetravalent titanium, the anhydrous oxides Ti_2O_3 and TiO_2 (rutile).] (Ref. 11)

27. $Ti \rightarrow Ti^{+3} + 3e \qquad E_o = - 1.21$

The standard potential for this reaction was based on $\Delta G° = 83.6$ k cal for Ti^{+3} ion (14). The phase boundary between Ti^{+3} and TiO is then

28. $Ti^{+3} + H_2O + e \rightarrow TiO + 2H^+ \qquad E^e = - 1.02 + 0.118$ pH

The effect of these changes on the potential - pH diagram is illustrated in Figs. 2 and 3 based on the anhydrous and hydrated oxides respectively.

The diagram considering both the hydride and the absence of the Ti^{+2} phase is shown in Fig. 4. The phase boundary Ti^{+3}/TiH_2 is given by:

29. $TiH_2 \rightarrow Ti^{+3} + 2H^+ + 5e \qquad E^e = - 0.81 - 0.024$ pH

based on the free energy of formation of TiH_2 used by Pourbaix (12) and equation 27.

It should be emphasized that the phase boundaries presented in the foregoing figures are for phases in thermodynamic equilibrium. In a real system under nonequilibrium conditions (as the freshly generated titanium surfaces) metastable phases may form within the phase fields of the stable species. These metastable phases may form when the kinetics for their formation is favorable but the kinetics for their reaction to the stable phase in that field is slow. An example of such a metastable phase field boundary that will be considered in the oxidation of freshly generated titanium surfaces is:

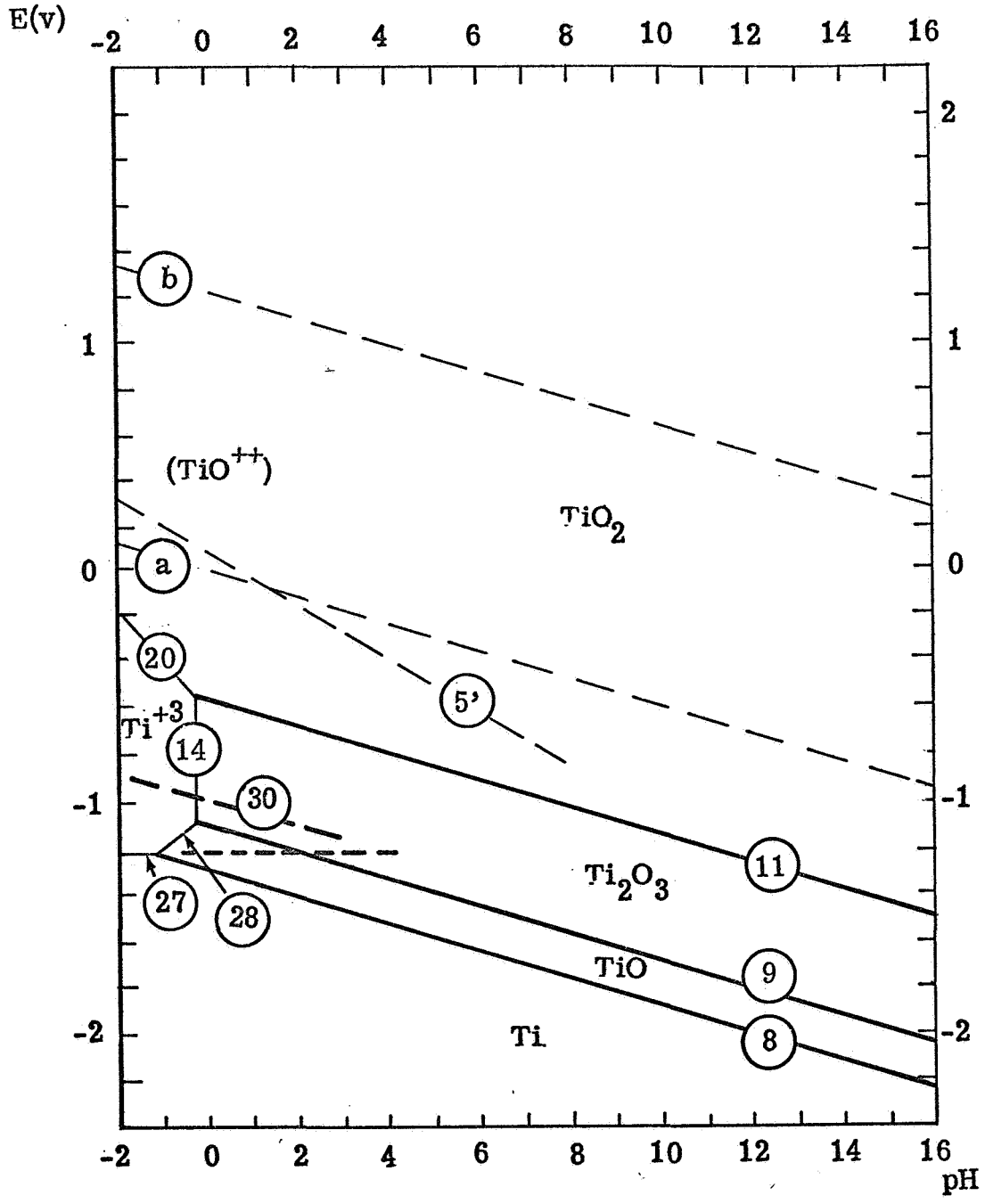

Fig. 2 Potential-pH equilibrium diagram for the system titanium-water, at 25°C. [Figure established by considering, as derivatives of tri- and tetravalent titanium, the anhydrous oxides Ti_2O_3 and TiO_2 (rutile).] (Modified re Ti^{+3})

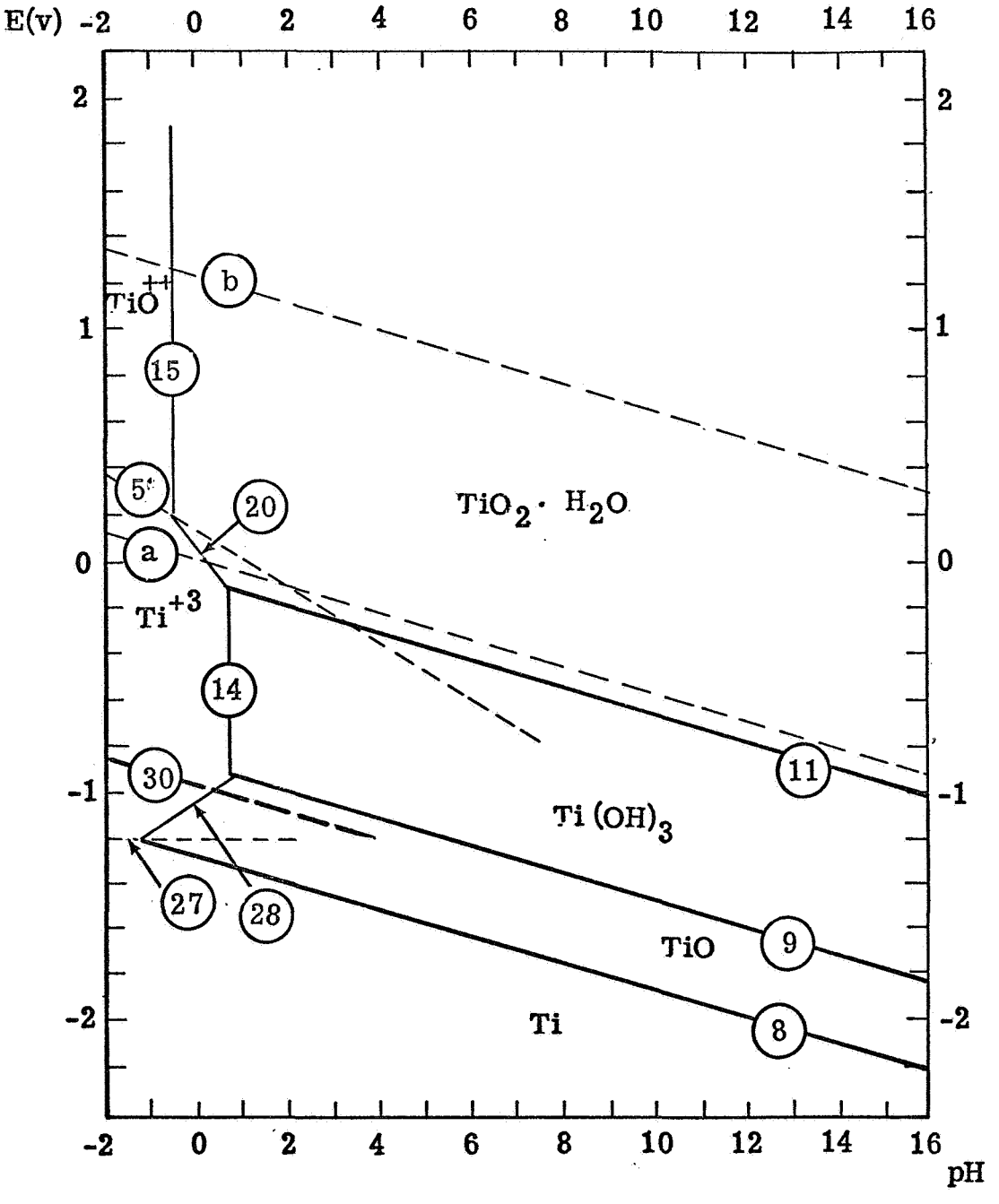

Fig. 3 Potential-pH equilibrium diagram for the system titanium-water, at 25°C. [Figure established considering, as derivatives of tri- and tetravalent titanium, the hydroxide $Ti(OH)_3$ and the hydrated oxide $TiO_2.H_2O$.] (Modified re Ti^{+3})

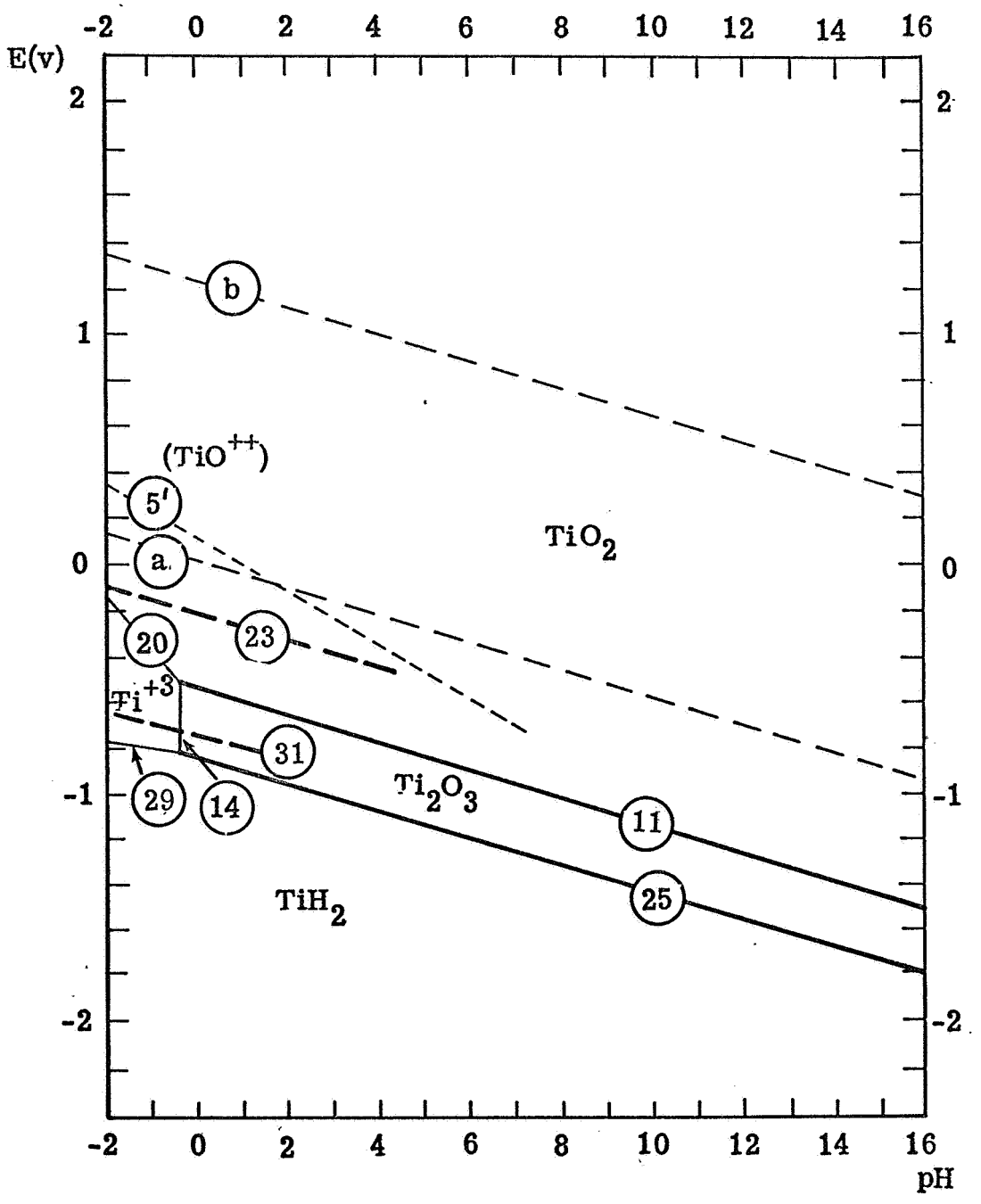

Fig. 4 Potential-pH equilibrium diagram for the system titanium-water, at 25°C. [Figure established by considering, as derivatives of tri- and tetravalent titanium, the anhydrous oxides Ti_2O_3 and TiO_2 (rutile).] (Modified re TiH_2 and Ti^{+3})

30. $Ti + 2H_2O \rightarrow TiO_2 + 4H^+ + 4e \qquad E^e = -0.98 - 0.059\ pH$

based on $\Delta G^\circ = -203.8$ Kcal for TiO_2 from Latimer (14). This is indicated as the heavy dashed line in Figs. 2 and 3. In the hydride system of Fig. 4 the corresponding boundary is:

31. $TiH_2 + 2H_2O \rightarrow TiO_2 + 6H^+ + 6e \qquad E^e = -0.73 - 0.059\ pH$

It is necessary to consider such reactions as 30 and 31 because titanium is to a large extent passivated even in concentrated HCl solutions.

An example of the sort of potential - pH path expected in a crack based on the MTK model (6) is shown in Fig. 5. The tip will tend to go to the mixed potential for oxidation of titanium (Reactions 27 and 30) and hydrogen ion reduction in acid solution. The acid concentration at first increases downstream from the tip and then decreases to pH = 7 at the mouth of the crack in neutral solution. Potentials applied at the mouth of the crack in the range of the linear velocity relationship vary from about -0.6 to + 1.2 V (SHE) (6).

The example path traverses the domains where the following species are stable or metastable:

Ti^{+3}, TiO_2, H_2, TiH_2

Ti_2O_3 or $Ti(OH)_3$

TiO_2 and TiO^{++}

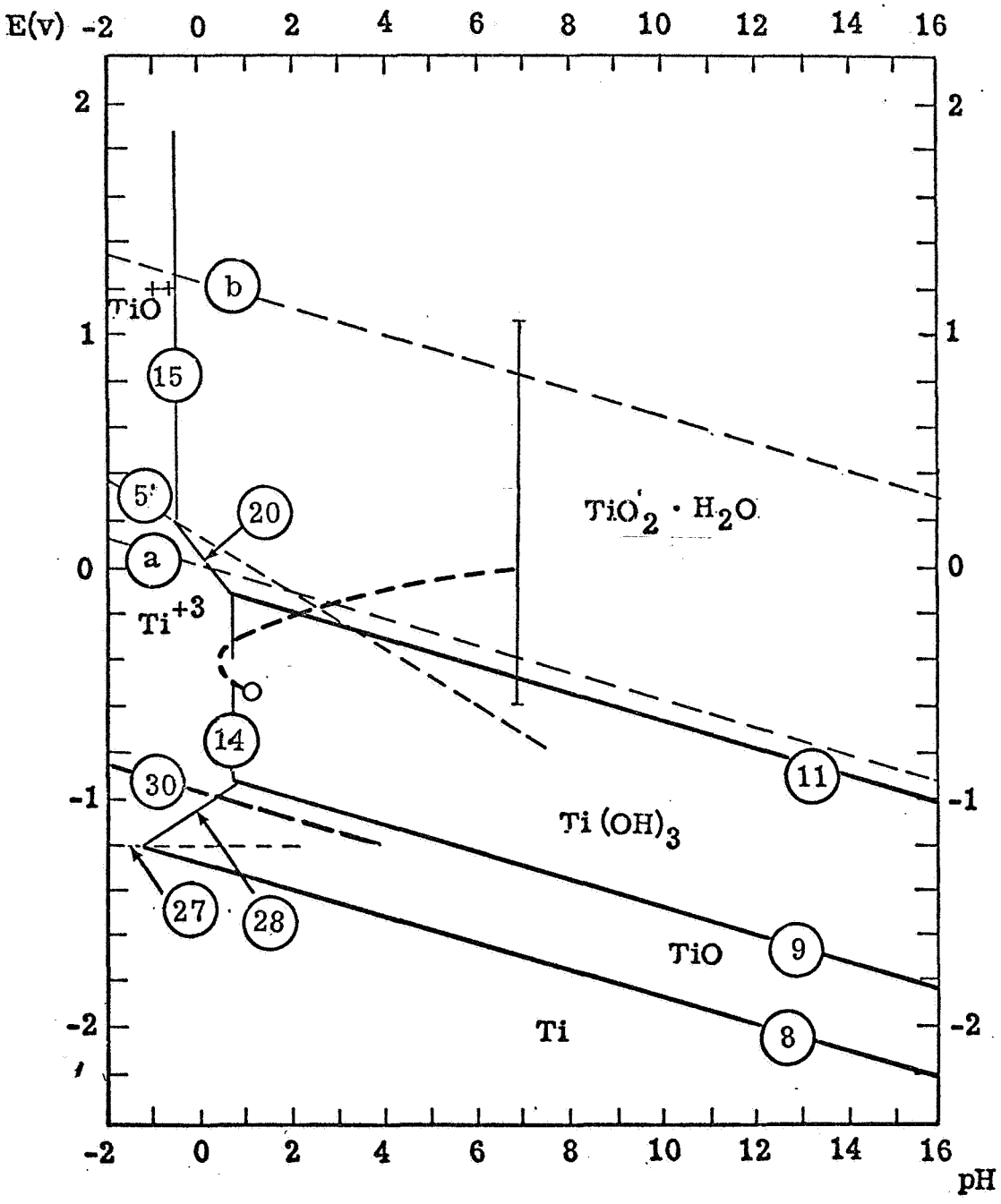

Fig. 5 Potential-pH path in stress corrosion crack

In order to make the analysis of the kinetic data possible, the only oxidized species that will be considered are Ti^{+3} in solution and TiO_2 film on the metal surface (the Ti^{+3}/TiO^{++} couple is considered under special circumstances). The current for the reduced species, H_2 and TiH_2 will for the most part have to be lumped because there is no definitive way of separating them yet.

3.1.2 Kinetics

The use of Tafel kinetics for hydrogen ion reduction and growth of the first monolayer of oxide and high field kinetics for growth of multilayers of oxide in the MTK model has been discussed (4). A point that requires further elaboration (appropriate to the more recent reexamination of the kinetic data) is the growth of the initial oxide layer.

In the MTK model it was assumed that the first monolayer of oxide could grow randomly on the surface so that coverage

$$d\theta = \frac{i d\tau}{Q_o} \qquad (3.1 - 1)$$

and

$$i = i_o(1-\theta) \exp\left(\frac{\alpha n F \eta}{RT}\right) \qquad (3.1 - 2)$$

leading at constant potential to

$$\theta = 1 - \exp(-\tau/\tau_1) \qquad (3.1 - 3)$$

and

$$i = i_1 \exp(-\tau/\tau_1) \qquad (3.1 - 4)$$

where $i_1 = i_o \exp\left(\frac{\alpha n F \eta}{RT}\right)$, $\tau_1 = Q_o/i_1$, i = current density, i_o = exchange current density, τ = time, Q_o = charge density of a monolayer, and the quantities in the exponential term have the usual significance.

Another mode of film growth, treated by Vermilyea (15), is peripheral growth of patches of oxide at a constant current density, i_2, on their peripheries. Treatment of this case leads to:

$$\theta = 1 - \exp\left[-n\pi\left(\frac{i_2\delta_m}{Q_o}\right)^2 \tau^2\right] \qquad (3.1 - 5)$$

and

$$i = \frac{2mn\pi i_2^2 \delta_m^2 \tau}{Q_o} \exp\left[-n\pi\left(\frac{i_2\delta_m}{Q_o}\right)^2 \tau^2\right] \qquad (3.1 - 6)$$

where m = number of monolayers in a patch, n = number of patches per cm^2 and δ_m = thickness of a monolayer in cm.

The kinetic data for hydrogen ion reduction on and oxidation of new titanium surfaces will be reviewed with respect to these two modes of film growth.

3.2 Rotating Disk and Ring-Disk Experiments

Two sets of experiments were conducted for the purpose of determining if soluble Ti^{+3} is formed in parallel with formation of oxide on new titanium surface in acid solution. The first was with a rotating titanium disk that was scraped with a sapphire cutting tool and the soluble titanium was determined colorimetrically using the hydrogen peroxide method (16). In the second set of experiments a titanium disk was scraped with a sapphire cutter and soluble Ti^{+3} formed was determined by oxidation to TiO^{+2} at a gold ring.

3.2.1 Rotating Disk Experiments

The geometry of the rotating disk experiments is illustrated in Fig. 6. The iodide-titanium rod (A.D. Mackay, New York) was bored out so that the area of the scraped face would not change as titanium was removed. A minimum volume of electrolyte ($\sim 20 m\ell$) was used so that a measurable concentration could be built up with a reasonable amount of scraping on the titanium. The table holding the cell and cutter was equipped with a motor drive for advancing the cutter into the rotating titanium tube. The titanium tube was potentiostated during the runs.

Soluble titanium was determined by the hydrogen peroxide method described in Kolthoff and Elving (16) using a Cary Model-14 Recording Spectrophotometer. A calibration curve was made according to the method of reference 16 using Bakers reagent grade TiO_2 as standard.

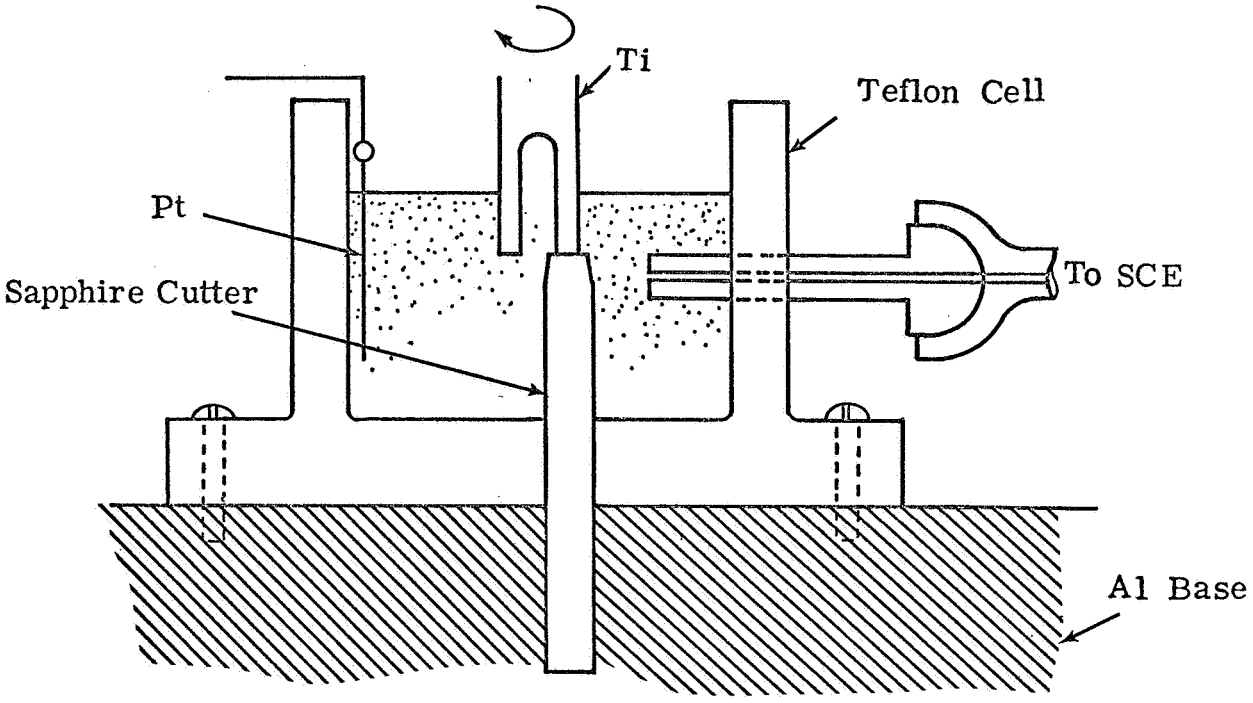

Fig. 6 Scraped titanium disk experiment

In the determinations, the soluble Ti^{+3} is oxidized to TiO^{+2} by the hydrogen peroxide to form a yellow colored complex with the excess of hydrogen peroxide.

At the completion of a run the electrolyte was poured out of the cell into a graduated cylinder and 3 cm^3 of 3% H_2O_2 was added and the total volume recorded. A portion of this solution was examined in the spectraphotometer. It was necessary to transfer the solution out of the cell rapidly after the run because the metal cuttings appeared to continue to react as evidenced by visible hydrogen evolution. Whether the cuttings were more active due to the large amount of cold working or whether the reactivity was due to the greatly increased surface is not known. The solution was a light violet color at the end of a run, indicative of Ti^{+3}.

Data for the runs are given in Table I. After the first run the same time was used for each in an effort to make the amount of dissolution of cuttings uniform. The weight of metal that would be dissolved if all of the charge passed was used to produce Ti^{+3} is indicated as W_1 in Table I. The weight of metal in solution corresponding to the spectrophotometric analysis is indicated as W_2. It may be noted in all cases that the metal pickup was greater than can be accounted for by electrochemical dissolution of the new surface, indicating considerable contribution from dissolution of the cuttings.

Run	1	2	3	4	5
Potential (mv)	0	0	+1000	O.C. (-800to-880)	-850
Time(sec)	64	124	124	125	125
Avg. Current (ma)	4.08	4.05	5.64	0	Cathodic
Q (amp sec)	0.261	0.502	0.700	0	-
W_1 (gm x 10^4)	0.43	0.83	1.16	-	-
Soln. vol. (cm^3)	20.0	23.0	19.5	16.8	20.3
ppm Ti^{+4}	10.	11.4	11.1	6.3	9.0
W_2 (gm x 10^4)	2.0	2.62	2.17	1.06	1.83
W_2-W_1 (gm x 10^4)	1.57	1.79	1.01	1.06	1.83
Ratio W_1:W_2	0.274	0.316	0.535	0	0

Table 1 Data for Scraped Ti Disk Experiments (~1000 RPM)

The data on dissolution of titanium are plotted in Fig. 7. Although there is a considerable amount of scatter, the data can be interpreted as shown as a linear increase in titanium dissolution with increased anodic potential and a constant background due to dissolution of the cuttings. The ratio, W_1/W_2, plotted in the upper part of Fig. 7 shows somewhat less scatter. The dashed curve is based on the two lines in the lower part of the figure;

$$\left(W_1/W_2\right)_{calc.} = \frac{W_1}{W_1+1.4} = \frac{(E+850)\left(\frac{0.8}{1000}\right)}{(E+850)\left(\frac{0.8}{1000}\right)+ 1.4} \qquad (3.2 - 1)$$

It was concluded from these experiments that a large fraction of the current to a new titanium surface goes to form soluble Ti^{+3} in acid solution but that more sensitive experiments would have to be devised to separate the component of current going to oxide formation.

Before describing the ring-disk experiments a brief analysis of the current in the scraping experiments will be given. The measured current versus potential from Table I is plotted in Fig. 8. The line drawn through the data was verified in independent experiments by varying the potential at the same constant advance rate on the cutter. The slope of the line gives a resistance of 270 ohms which is about six times larger than the value calculated from kinetics data for oxidation of new titanium surface in 12 M and 3 M HCl. The calculated current was obtained from

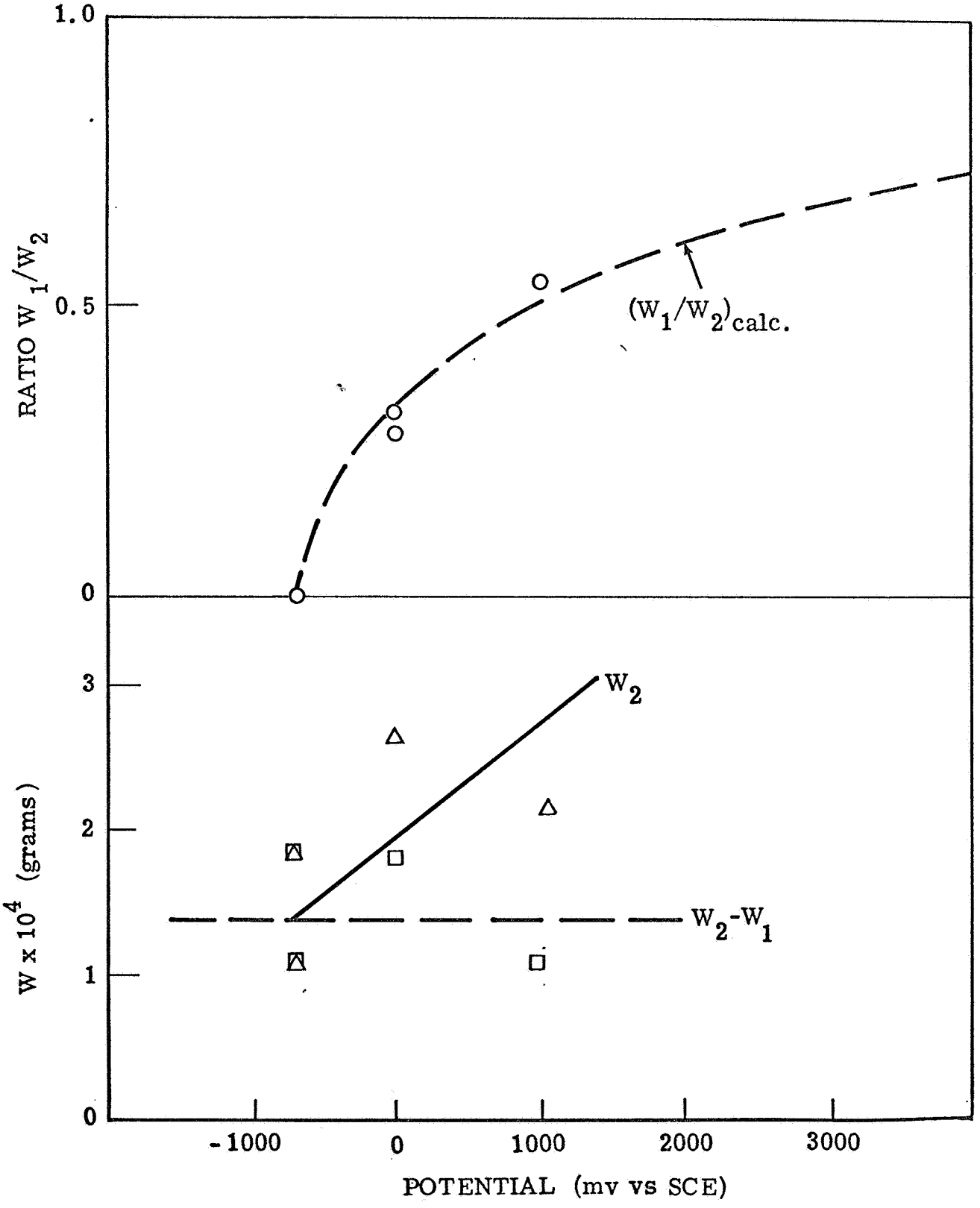

Fig. 7 Scraped Ti disk experiments in 6M HCl at ~1000 RPM - weight of Titanium in solution

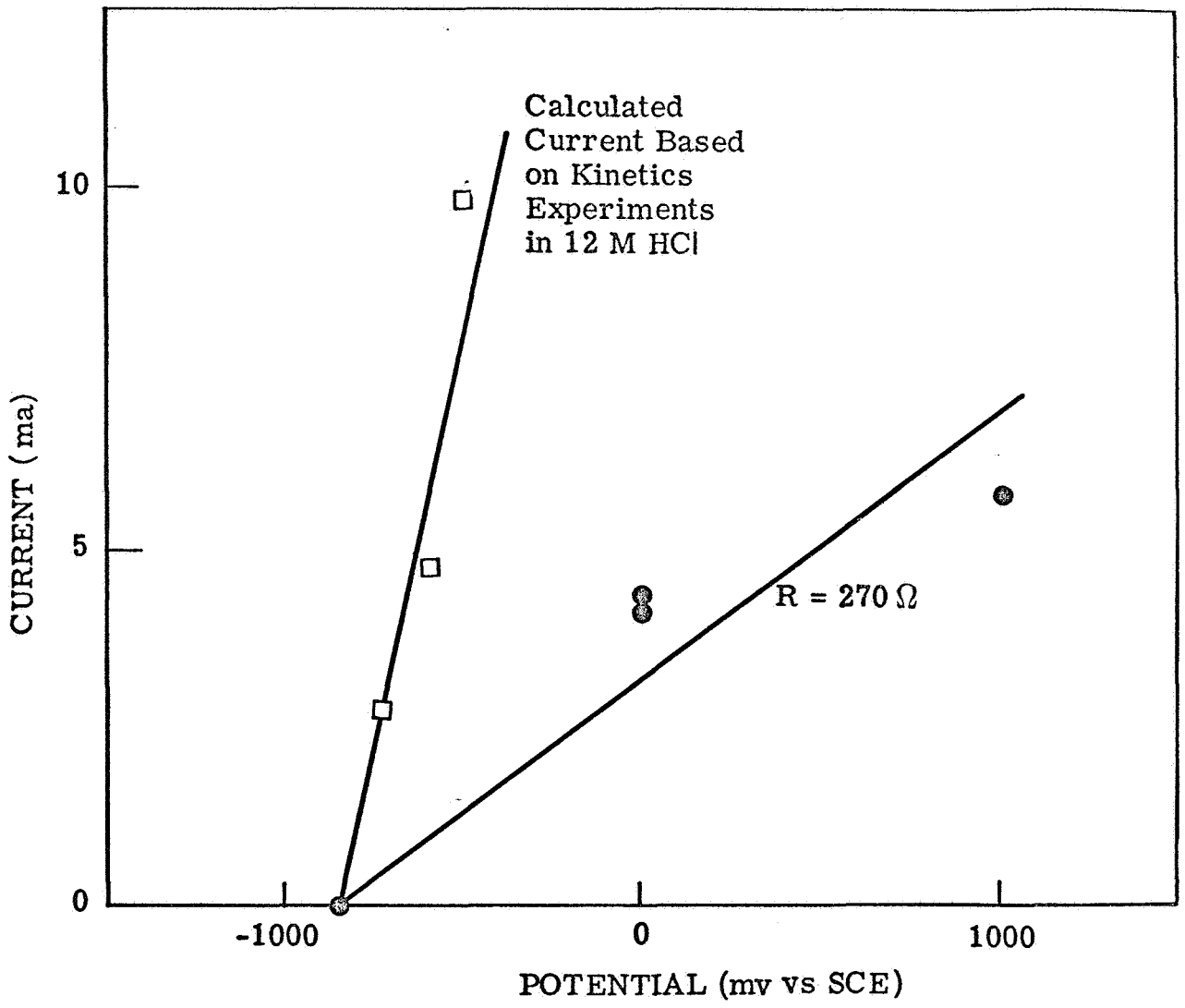

Fig. 8 Current - Potential curve for scraped Titanium disk experiment in 6M HCl at ~1000 RPM

$$\bar{I} = \frac{A \int_0^{\tau_r} i \, d\tau}{\tau_r} \qquad (3.2 \text{ -2})$$

where A = scraped area of disk (0.16 cm^2), τ_r = time between cuts. (0.060 sec for 1000 RPM), and $id\tau$ is the integral of the current density versus time data from the kinetics experiments. Further analysis and experiments showed that the current in the scraping experiments was low because the depth of cut was small compared to the radius of the cutting edge, resulting in a stick-slip condition.

The effect of tool advance rate on current is shown in Fig. 9. The current appears to become asymptotic to a limiting value at the higher advance rates, where the depth of cut approached a micron at a speed of 1000 RPM. There was still a considerable amount of stick-slip even at the higher advance rates as evidenced by tool chatter. This is not surprising in view of the radius of the cutting edge of the tool being on the order of 10^{-3} cm and an average depth of cut being less than 10^{-4} cm. The data in Table 1 were obtained with an average advance rate of 2 mils/min. so the low current is in large part due to sporadic cutting associated with the stick-slip phenomenon. This was also reflected in the very erratic current during the runs.

At a given advance rate the current increased with rotational speed as shown in Fig. 9. This is the result of the decrease in τ_r and its influence on $\bar{I}$ as indicated by equation 3.2 - 2. Equation 3.2 - 2 may be rewritten to give

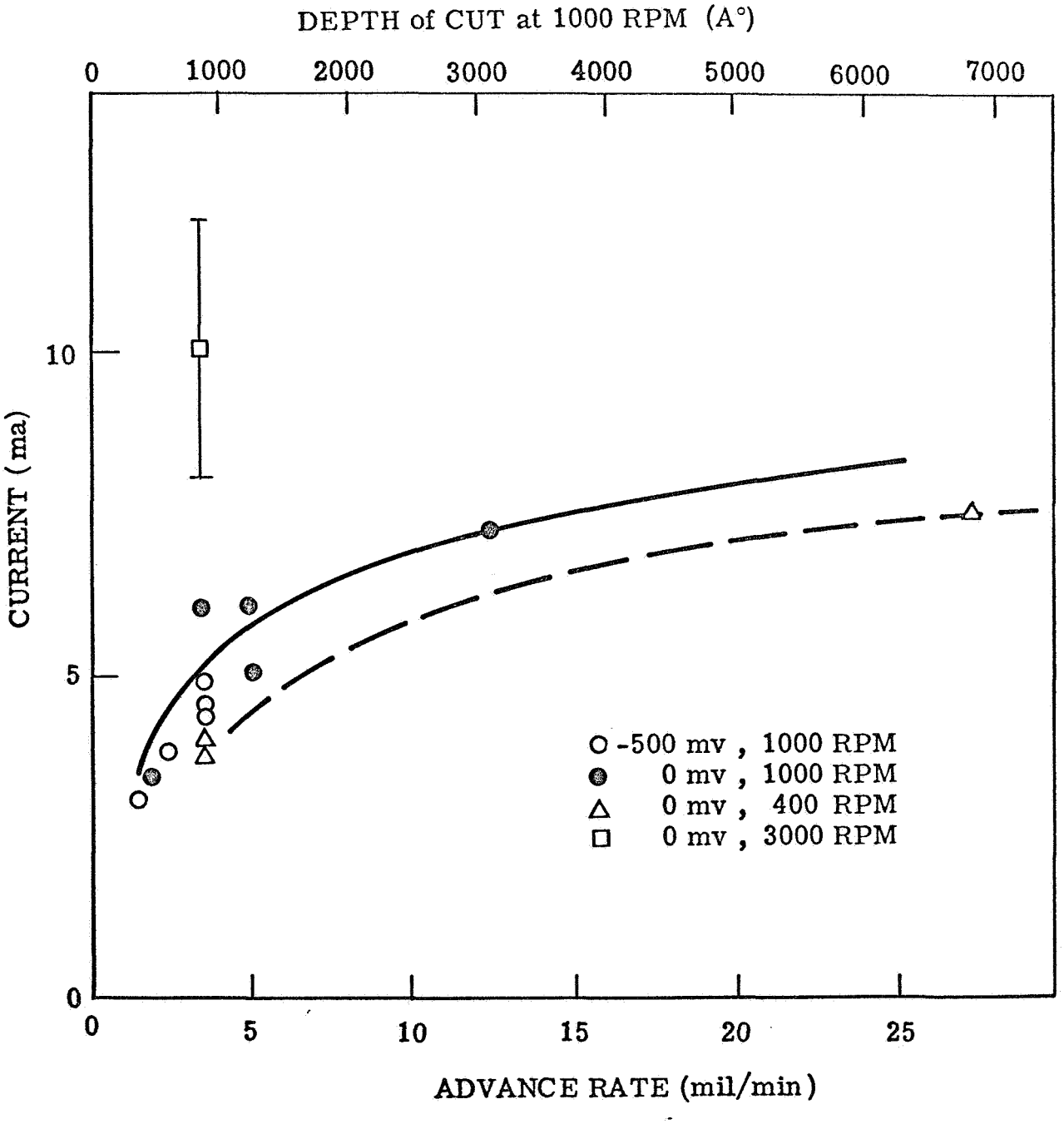

Fig. 9 Effect of tool advance rate on current

$$f = \frac{60}{AQ} \left[\frac{\bar{I}}{(RPM)}\right] \qquad (3.2 - 3)$$

where f = fraction of new metal surface created per revolution and $Q = \int_0^{\tau_r} i \, d\tau$. It turns out that in the kinetics experiments the current became negligible after about 15 milliseconds and the value of Q became essentially constant. Values of Q found in 12 M and 3 M HCl at a potential of 0 mv SCE were 7.6×10^{-3} coul/cm^2 and 6.0×10^{-3} coul/cm^2 respectively. An average value of 6.8×10^{-3} coul/cm^2 will be assumed for the 6 M HCl in the scraping experiments. The value of τ_r is 20 milliseconds at 3000 RPM to 150 milliseconds at 400 RPM so use of a constant value of Q appears justified in equation 3.2 - 3. The value of f varied from 0.19 for the run at a 2 mil/min advance rate and 1000 RPM (typical of conditions in Table I and Fig. 7) to 1.03 for the run with a 27 mil/min advance rate and 400 RPM. The latter value indicates complete oxide removal per cut of 1.7 microns depth.

3.2.2 Ring Disk Experiments

The design of the Ring-Disk electrode is shown in Fig. 10. The gold ring and titanium rod of which the exposed end formed the disk were mounted in a Teflon body in turn fastened to the rotating shaft through a screw fitting. The disk material was iodide titanium as in the scraped disk experiments and the ring was gold of 99.9% purity. Leads from the disk and ring were connected

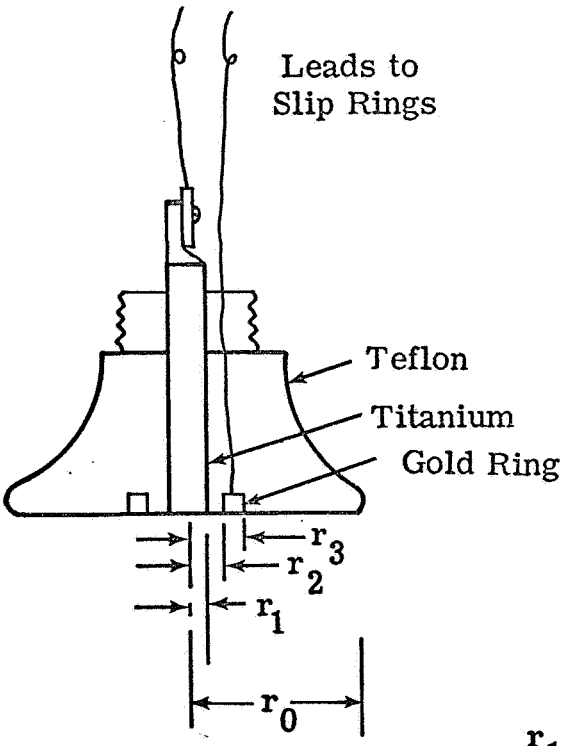

$r_1 = 0.25$ cm
$r_2 = 0.30$ cm
$r_3 = 0.45$ cm
$r_0 = 2.0$ cm

Fig. 10 Design of ring-disk electrode

through a Huttinger Baldwin Messtechnik SK-6 slip-ring assembly to the external circuit (four slip rings connected to the disk and two slip rings connected to the ring).

The electrode was operated in a square Plexiglas cell with internal dimensions S = 10 cm and H = 8 cm, filled to 6 cm, with electrolyte. The disk was potentiostated, the saturated calomel reference electrode at the edge of the Teflon body and the platinum counter electrode at the side of the cell as indicated in Fig. 11. A silver sheet anodized in chloride solution with 3 1/2 cm by 18 cm immersed area (per side) was used as the reference and counter electrode for the gold ring. A bias voltage was applied to the gold ring with a 100 ohm potentiometer across two mercury cells, and a 10 ohm shunt was used for measuring current. The disk was scraped by a sapphire cutter mounted on a titanium holder attached to the bottom of the cell.

Before the scraping experiment could be interpreted a number of preliminary experiments and calibrations had to be made. These included measurement of polarization curves for oxidation of Ti^{+3} on gold, determination of the ring efficiency for reduction of iodine and oxidation of Ti^{+3} generated at the disk, determination of ring current for hydrogen generated at the disk, study of ring transients and the effect of the scraper or ring current.

The irreversibility of the Ti^{+3}/TiO^{+2} couple in polarography on a mercury surface is well known (17). A similar irreversibility has

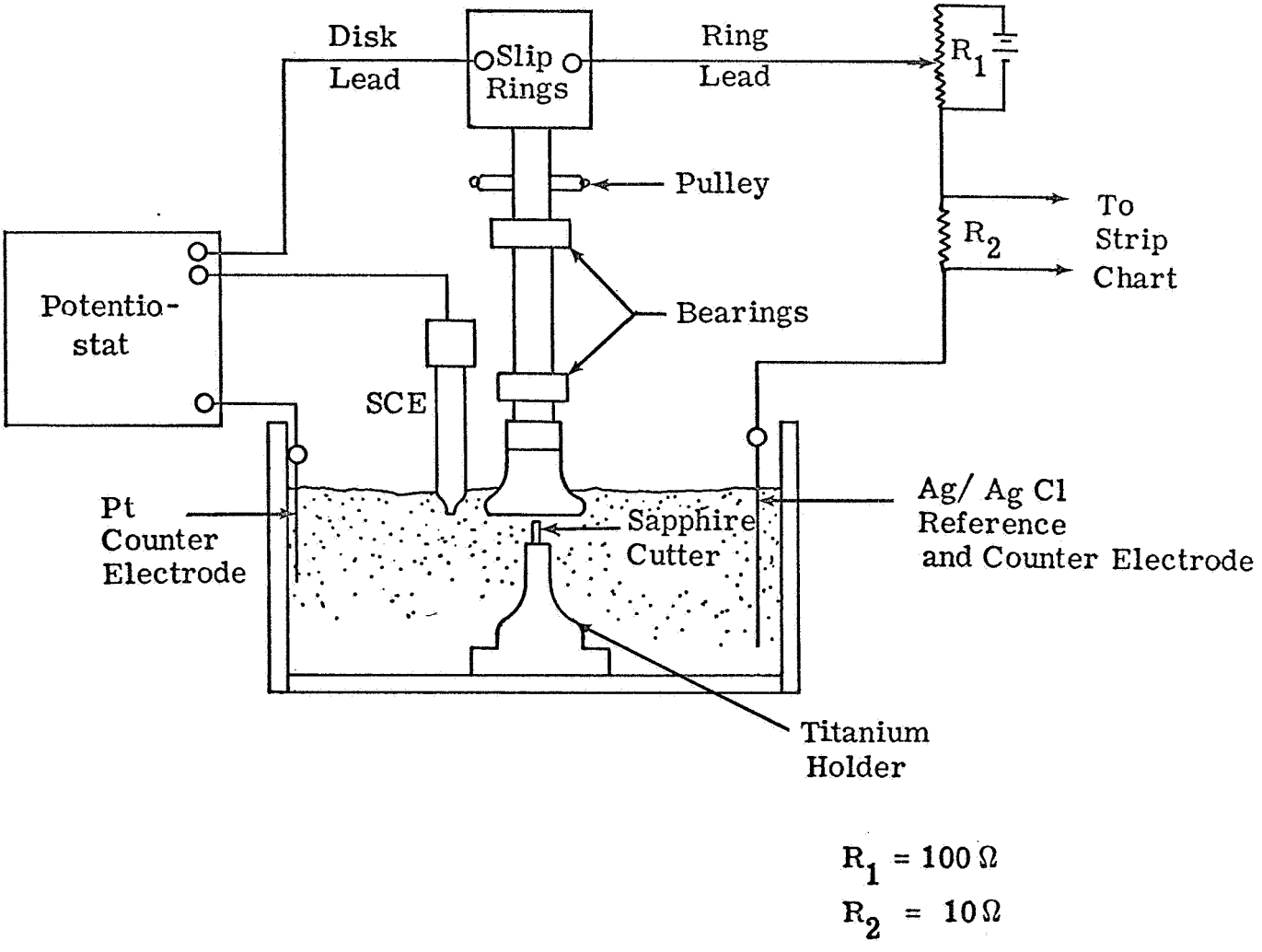

Fig. 11 Physical arrangement of cell and electrical circuits

been observed in the present work on gold and platinum electrodes. The couple is so irreversible that no oxidation current was measured with a 0.1 M $TiCl_3$ solution between the potentials of hydrogen and oxygen evolution. The standard reversible potential of the couple given by Latimer (14) is about + 0.1 V (SHE, Stockholm convention) or about - 140 mv vs. SCE.

In agreement with the polarographic work (17), an oxidation current was found with a gold electrode in a solution of 0.1 M $TiCl_3$ in .6 M HCl as indicated in Fig. 12. (Curve A is for 6 M HCl and the anodic current at ~+700 mv is dissolution of gold. According to Latimer (14) the standard potential for formation of the $AuCl_4^-$ complex is + 1.0 volt (SHE) or + 760 mv SCE. The equilibrium potential should be approximately 60 mv less positive in 6 M HCl. The cathodic current at -200 mv is for hydrogen evolution.) The anodic part of curve B is for oxidation of Ti^{+3}. At a potential above + 250 mv the current becomes limited by diffusion as evidenced by a considerable increase in current when the electrolyte is stirred. The steady-state limiting current density is $\sim 0.5 \times 10^{-3}$ amp/2.5 cm^2 = 2×10^{-4} amp/cm^2 (but $\sim 10^{-3}$ amp/cm^2 in a later experiment) compared to a calculated value of 2×10^{-3} amp/cm^2 for a diffusivity of 10^{-5} cm^2/sec and a diffusion layer thickness of 5×10^{-2} cm for a one-electron reaction. The reversible potential for the Ti^{+3}/TiO^{+2} couple appears to be between -50 and -130 mv in approximate agreement with the value from Latimer (14) but the value is influenced to some extent by hydrogen

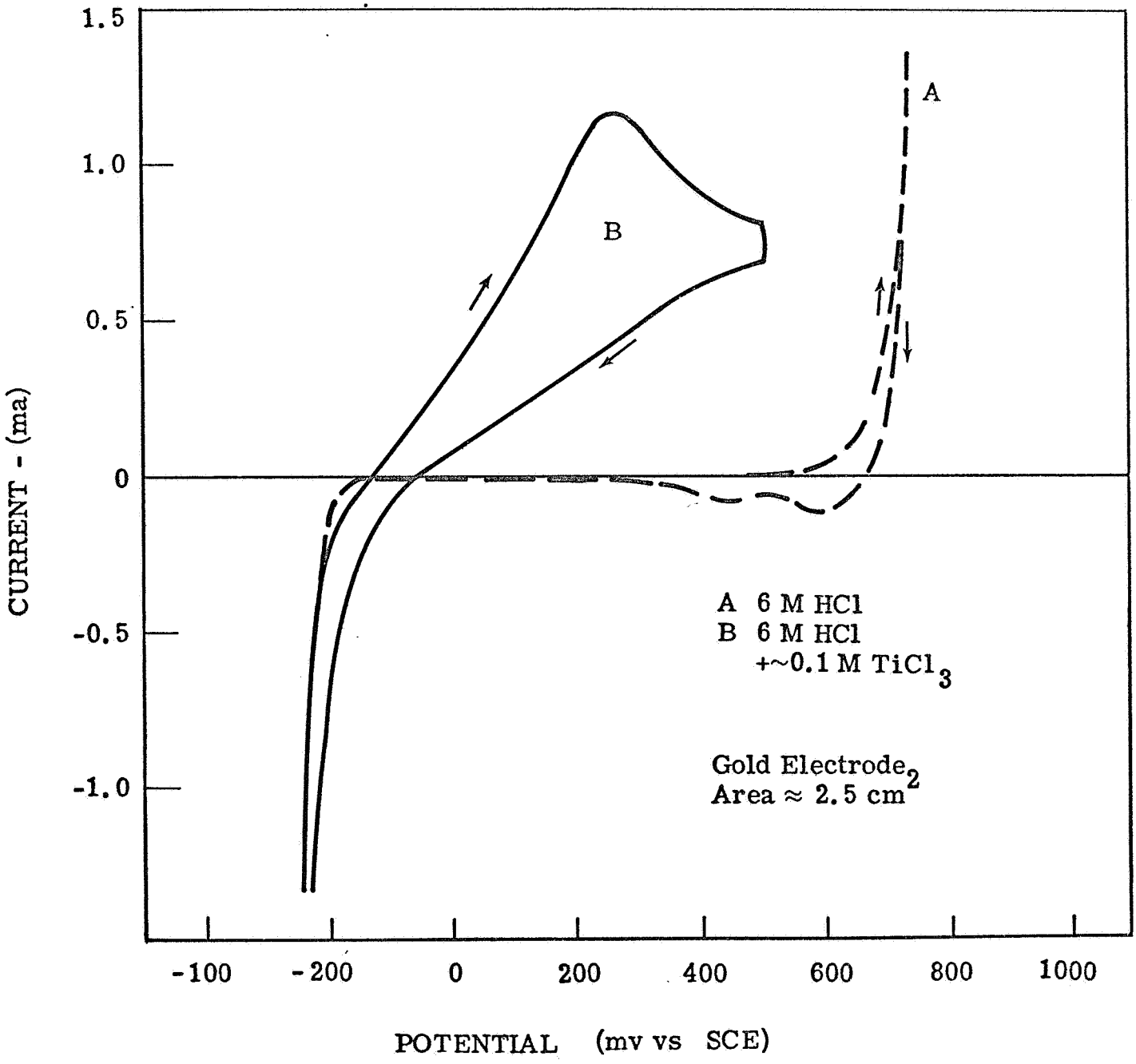

Fig. 12 Polarization curve of gold electrode in 6M HCl and 6M HCl + 0.1 M $TiCl_3$ (sweep speed 624 mv/min.)

evolution. In spite of the high concentration of HCl there still exists a high degree of irreversibility for oxidation of Ti^{+3} as evidenced by the slow rise in current with potential up to 250 mv.

The efficiency of the ring for oxidation of Ti^{+3} produced at the disk was determined by reducing TiO^{+2} from solution on the disk and reoxidizing the Ti^{+3} at the ring. The electrolyte was approximately 0.4 M TiO^{+2} in 6 M HCl, produced by dissolving Bakers reagent grade $TiCl_4$ in concentrated HCl and diluting to 6M. The titanium disk was at -250 mv (SCE) for reduction of TiO^{+2} and the gold ring potential was varied from +100 to +800 mv versus the Ag/AgCl electrode (Ag/AgCl electrode was -118 mv to SCE in 6M HCl). Hydrogen overvoltage is greater on titanium than on gold so essentially all of the current to the disk at -250 mv went to reduction of TiO^{++}.

Efficiency of Ti^{+3} oxidation versus potential at the ring is given in Table 2 and plotted in Fig. 13 for a rotational velocity of 400 RPM. Efficiency was calculated from

$$N = \Delta I_R / I_D \qquad (3.2 - 4)$$

where ΔI_R is the change in ring current (anodic) with cathodic disk current. It may be noted that a high degree of irreversibility for oxidation of Ti^{+3} at the ring is indicated by the low efficiencies

E_{Ring} (mv vs Ag/AgCl	I_{Disk} (ma) (cathodic)	ΔI_{Ring} (ma) (Anodic)	N
+ 100	3.20	0.11	0.035
100	3.22	0.078	0.024
100	2.55	0.050	0.020
100	3.30	0.056	0.017
200	2.50	0.102	0.041
200	3.00	0.112	0.037
300	3.30	0.267	0.081
300	3.00	0.188	0.062
400	3.00	0.373	0.124
400	3.00	0.340	0.113
500	3.50	0.650	0.185
600	3.50	0.950	0.272
700	3.50	1.20	0.343
800	4.00	0.475	0.119
600	4.00	1.55	0.388
400	4.00	1.04	0.260
200	4.47	0.330	0.074

Table 2 Disk and Ring Current and Ring Efficiency for Oxidation of Ti^{+3} Generated at Disk by Reduction of TiO^{++} in 0.4 M TiO^{++} in 6 M HCl

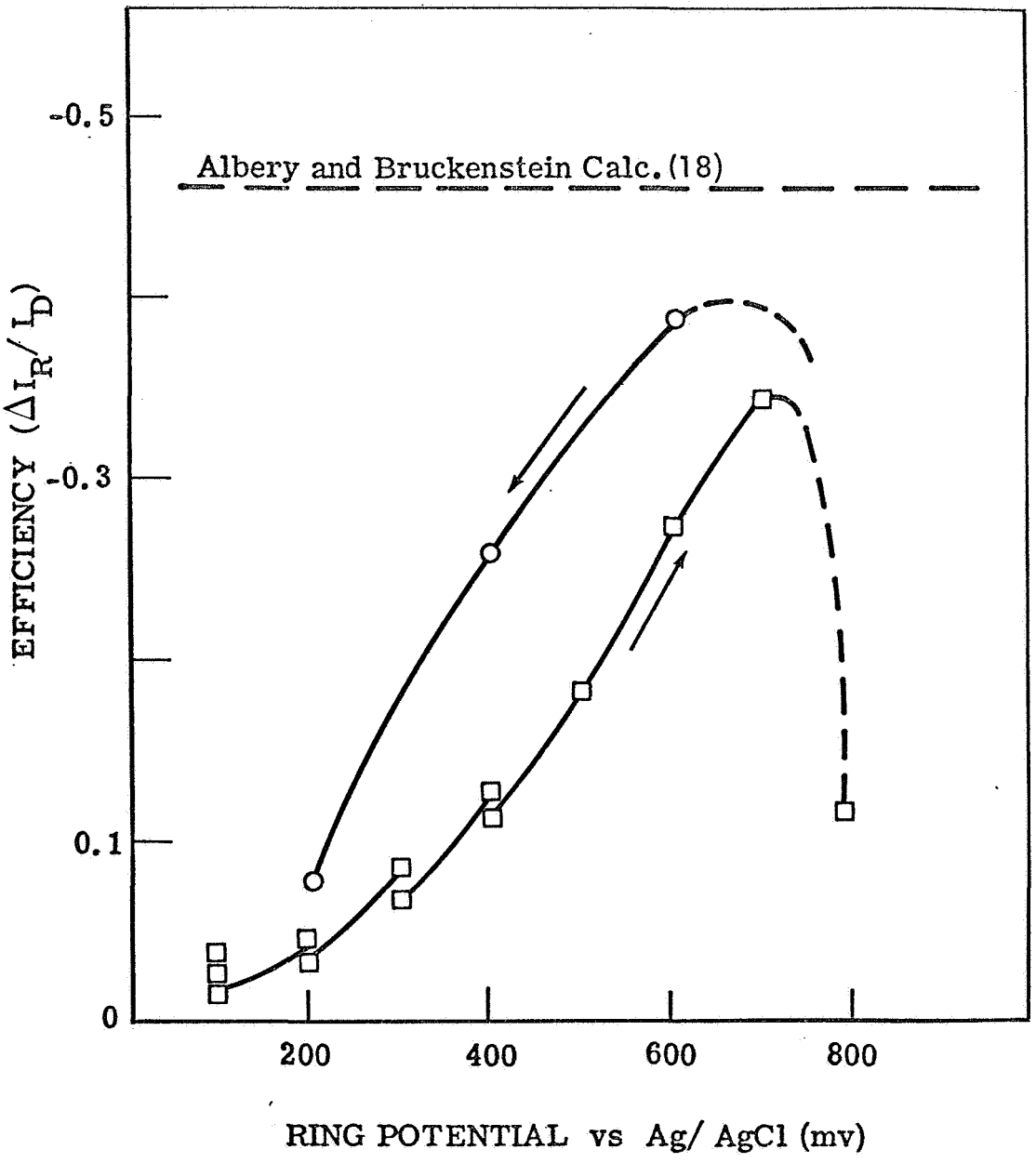

Fig. 13 Ring efficiency for oxidation of Ti^{+3} generated for oxidation of Ti^{+3} generated at disk by reduction of TiO^{++} in 0.4 M TiO^{++} in 6M HCl

compared to the value extrapolated from the Albery and Bruckenstein model (18) for the ring and disk dimensions given in Fig. 10. Furthermore, at a given ring potential the efficiency decreased with time indicating a poisoning of the surface. The efficiency was also higher after the ring had been to a potential of +800 mv vs Ag/AgCl where gold dissolution occurred and the surface was evidently partially cleaned of the poisoning agent. As indicated in Fig. 2, TiO_2 is a likely species that could form on the surface from oxidation of Ti^{+3} to TiO^{+2}. If this is indeed true the technique might be modified to study oxidation of Ti^{+3} to TiO_2.

Because of the low ring efficiencies observed in the oxidation of Ti^{+3} at the ring it was desirable to check the Albery and Bruckenstein model (18) against a more reversible couple. The I^-/I_2 couple was studied in neutral 0.6M KI solution; I^- being oxidized at the disk to I_2 and the product I_2 reduced at the ring. Data are presented in Table 3. The average ring efficiency at 400 RPM of 0.44 is close to the value of 0.46 from Albery and Bruckenstein (18). It is not known whey the ring efficiency decreased with increase in RPM; Levich (19) and Albery and Bruckenstein (18) show that N should be independent of rotation speed. Ring efficiency was essentially independent of disk and ring currents and of ring potential from -100 mv to nearly +500 mv to the Ag/AgCl electrode showing that the ring current was indeed under diffusion control. The decrease in efficiency at a ring potential of 580 mv vs Ag/AgCl

RPM	E_{Disk} (mv-SCE)	E_{Ring} (mv-Ag/AgCl)	I_{Disk} (ma) (anodic)	I_{Ring} (ma) (cathodic - anodic +)	ΔI_{Ring} (ma) (cathodic)	N	
400	660	0	4.30	-0.15	1.85	0.430	
400	580	0	1.85	-0.15	0.825	0.445	
400	520	0	0.85	-0.15	0.375	0.440	
						0.438	Avg.
1000	650	0	3.45	-0.15	1.44	0.417	
1000	600	0	1.95	-0.15	0.835	0.428	
1000	550	0	1.05	-0.15	0.440	0.418	
						0.421	Avg.
100	660	0	3.16	-0.15	1.49	0.471	
100	600	0	1.70	-0.15	0.82	0.482	
100	550	0	0.95	-0.15	0.45	0.474	
						0.476	Avg.
400	660	-100	2.75	-0.78	1.21	0.440	
400	600	-100	1.50	-0.78	0.675	0.450	
						0.445	Avg.
400	660	+200	2.50	+0.04	1.075	0.430	
400	600	+200	1.40	+0.04	0.625	0.445	
						0.438	Avg.
400	660	+300	2.43	+0.07	1.075	0.442	
400	660	+500	2.32	+0.35	1.00	0.431	
400	660	+580	2.27	+2.38	0.725	0.320	

Table 3. Calibration of Ring Efficiency in 0.6M KI Solution

was due to kinetic control of the reduction of I_2 near the reversible potential of the I^-/I_2 redox couple as indicated by the high background anodic current on the ring. It may be noted that at the same potential the anodic disk current decreased in successive experiments due to the increasing oxide thickness on the titanium. Scraping the disk restored the higher current. It was found that moving the sapphire scraper near the disk but not touching it had a negligible effect on the ring efficiency for these experiments.

The ring current and efficiency were determined for oxidation of hydrogen generated at a negative potential on the disk because of the possibility of error in the scraping experiments due to oxidation at the ring of hydrogen generated on the new surface and on the cuttings. The data shown in Table 4 indicate some anodic oxidation at the ring of dissolved hydrogen but the current and efficiency were small compared to the values for oxidation of Ti^{+3} shown in Table 2. Because the ring current is very small in relation to a large disk current in Table 4 it is assumed that oxidation of dissolved hydrogen can be neglected at the ring in the scraping experiments.

Ring and disk currents in several scraping experiments in 6M HCl are presented in Table 5. It was assumed that the ring current was essentially all for oxidation of Ti^{+3} to TiO^{+2}. The equivalent current at the disk to form the Ti^{+3} is therefore

I_{Disk} (ma) (cathodic)	ΔI_{Ring} (ma) (anodic)	N
140	0.07	0.0005
150	0.04	0.0003

Table 4 Ring Efficiency for Oxidation of Hydrogen Generated at Disk (Ring at +500 mv vs Ag/AgCl, Disk at -1400 mv SCE)

E_{Disk} (mv) (SCE)	E_{Ring} (mv) (Ag/AgCl)	ΔI_{Disk} (ma) (anodic)	ΔI_{Ring} (ma) (anodic)	N (Fig.13)	$\frac{3\Delta I_{Ring}}{N}$ (ma)	$\frac{3\Delta I_{Ring}}{N\Delta I_{Disk}}$
-500	+700	9.5	0.85	0.35	7.3	0.77
-500	+700	6.5	0.84	0.35	7.2	1.11
						0.94 Avg.
-300	+500	8	0.05	0.19	0.8	0.10
-300	+500	12	0.15	0.19	2.4	0.20
-300	+500	18	0.6	0.19	9.5	0.53

Table 5 Ring and Disk Currents in Scraping Experiments

(6 M HCl Electrolyte, 400 RPM Rotation Speed)

$$I = \frac{3\Delta I_{Ring}}{N} \qquad (3.2 - 5)$$

The ratio of this value to the change in disk current with scraping should give the fraction of the disk current to form soluble Ti^{+3} (there was some continuous background cathodic current for hydrogen ion reduction at the disk potentials in Table 5, thus the use of ΔI_{Disk}). In the first two experiments shown in Table 5 in which a relatively high tool advance rate was used, it appears that most of the disk current went to soluble Ti^{+3}. Of course, the value of N used from Fig. 13 is very approximate due to the poisoning of the ring so the experimental results are not very precise, but it is important that it has been demonstrated that a large fraction of the current to a new titanium surface in acid solution goes to form soluble Ti^{+3}.

In the last three experiments shown in Table 5 a lower but successively increasing tool advance rate was used. The ring current increased more with tool advance rate than the disk current suggesting that perhaps at low tool advance rates that TiO_2 is scraped off preferentially and most of the current goes to grow more oxide on the thinned oxide. Unfortunately only a limited number of scraping experiments was conducted with the ring disk system because the disk was damaged and had to be repaired after each set of experiments, particularly at the high cutting rates required.

During the scraping experiments it was observed that although an increase in anodic ring current occurred during scraping, there appeared to be no correlation between current peaks on the disk and ring when the "fine structure" was investigated on an expanded time scale. A reasonable explanation for this appeared to be that there is a delay time for transport of Ti^{+3} from disk to ring and that this delay time is variable depending on the radial position of transiently scraped patches of metal on the disk. Subsequent measurements made of the transport delay time from disk to ring were consistent with this hypothesis.

A strip chart record of disk and ring transient currents accompanying step changes in disk potential in 0.6M KI solution from an essentially zero I^- ion oxidation current to about 0.4 ma is shown in Fig. 14. It may be noted that at the instant the potential was switched on the disk, denoted by τ_p, there was a slight change in the ring current probably due to a change in IR drop in the solution near the electrode face. There was then a delay time denoted by $\Delta\tau_d$, between this time τ_p, and the onset of change in ring current due to reduction of I_2. The latter time was determined by extrapolating the initial-current slope back to the intersection with the pre-potential step current. (That $\Delta\tau_d$ is approximately equal to the time difference in the two pen positions is a coincidence in this experiment.) The same value of $\Delta\tau_d$ was

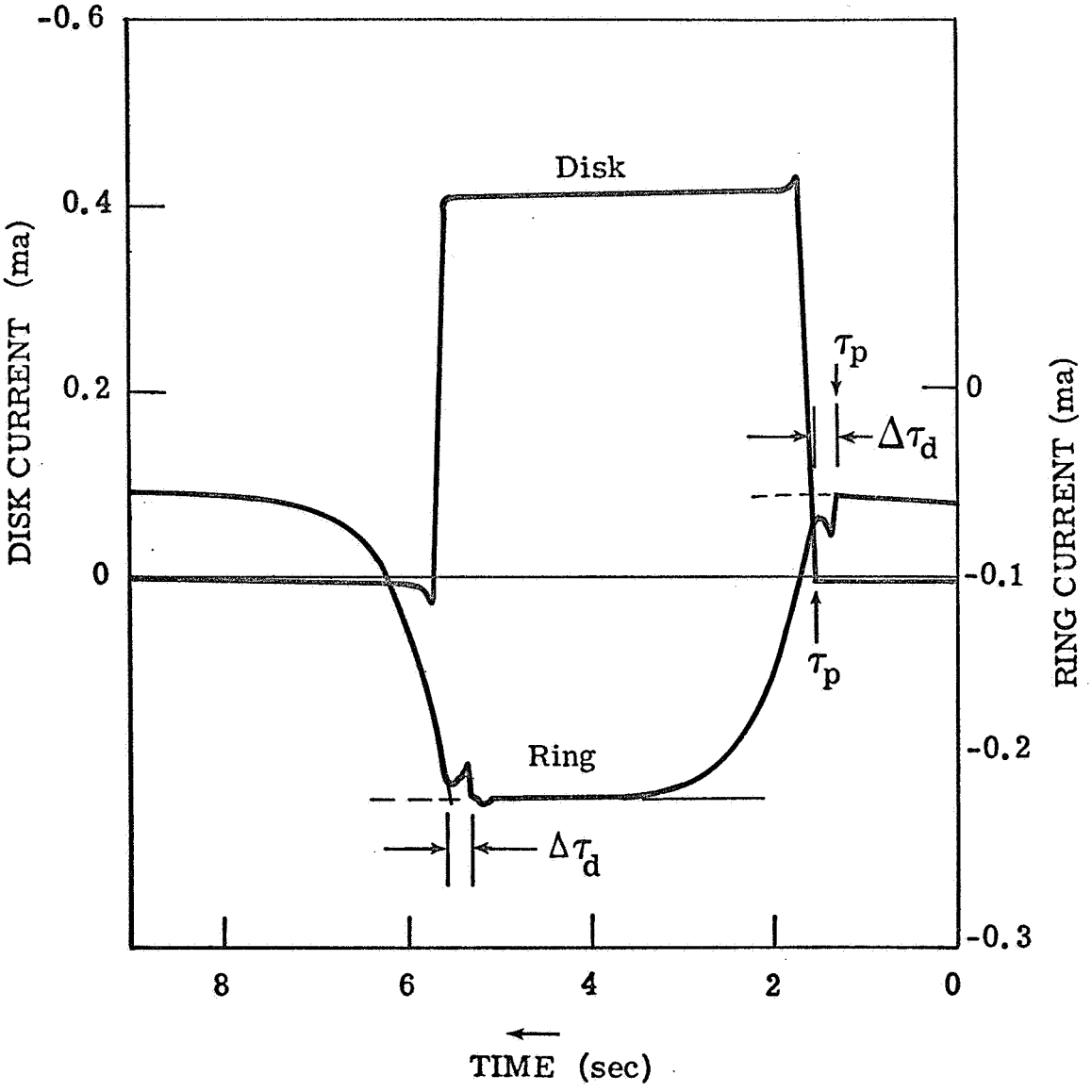

Fig. 14 Strip chart recording of disk and ring transient currents for step change in disk potential in 0.6M KI solution (400 RPM)

found for the potential step to the zero disk current and from zero to a finite disk current.

A plot of delay time versus the period of revolution for three speeds is given in Fig. 15. A linear relation passing through the origin was obtained. The delay time at 400 RPM, at which most of the ring-disk scraping experiments were done, is about 0.25 sec. This is for a gap between ring and disk of 0.05 cm (Fig. 10). The radial distance between the boundaries of the scraped zone on the disk and the inner radius of the ring was in the range of about 0.1 to 0.25 cm. Assuming constant radial velocity across this portion, the disk would therefore give delay times of 0.5 to 1.25 seconds, which would explain the lack of correlation of ring and disk current peaks at a high time resolution. The actual delay times would be longer than these because radial velocity of solution is a function of radius as discussed below.

It is of interest to examine the significance of the ring-disk delay time to the hydrodynamic equations for the rotating disk electrode. It can be shown from Levich (19) that the radial velocity in the solution next to the disk can be approximated by

$$v_r = 0.51\ \omega r \left(\frac{\omega}{\nu}\right)^{\frac{1}{2}} y \qquad (3.2 - 6)$$

where ω = rotational speed, radians/sec; r = radial position on disk, where the velocity v_r is determined; ν = kinematic viscosity;

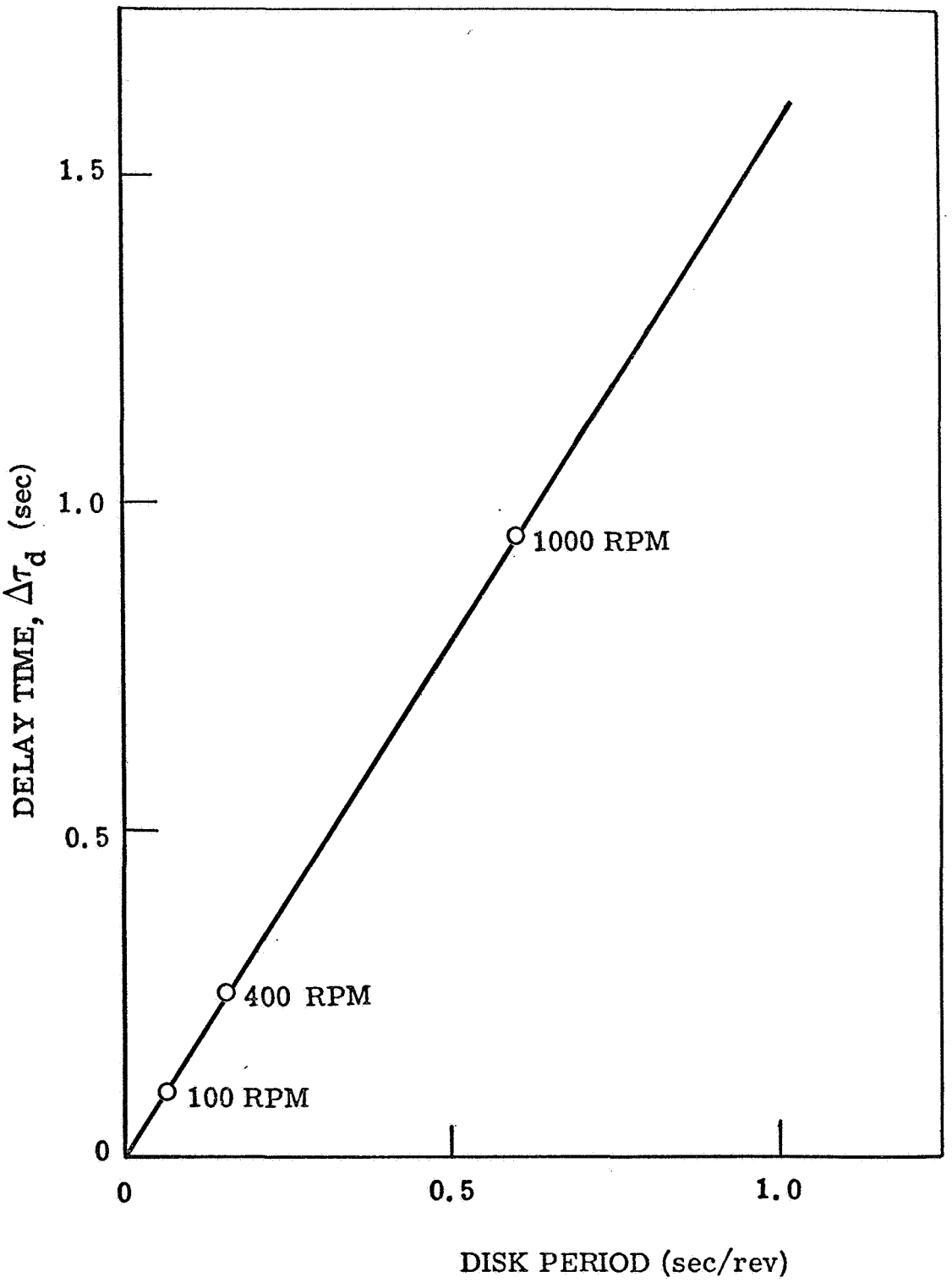

Fig. 15 Plot of delay time, $\Delta\tau d$, versus period of revolution

and y = distance into solution normal to disk. Because the radial solution velocity is zero at the disk surface, the delay time is the sum of the time for disk products to diffuse from r_1 (Fig. 10) to a position in the fluid y_d with finite velocity and be transported from r_1 to r_2 and finally to diffuse back to the ring at r_2 (Fig. 10). The value of y_d must be between zero and δ, the diffusion layer thickness.

The diffusion layer thickness (19) is given by

$$\delta = 1.61 \left(\frac{D}{\nu}\right)^{1/3} \left(\frac{\nu}{\omega}\right)^{1/2} \qquad (3.2 - 7)$$

where D = diffusivity of transported species. The ratio of y/δ from equations 3.2 - 6 and 3.2 - 7 is

$$y/\delta = \frac{v_r}{(0.82)\ \omega r \left(\frac{D}{\nu}\right)^{1/3}} \qquad (3.2 - 8)$$

The value of v_r is given approximately by

$$v_r \geq \frac{r_2 - r_1}{\Delta\tau_d} \qquad (3.2 - 9)$$

the value of v_r being larger than the right hand side because $\Delta\tau_d$ contains the diffusion times as well as the convection time from r_1 to r_2. Empirically it is found from Fig. 15 that

$$\Delta\tau_d = 1.60 \left(\frac{60}{RPM}\right) \qquad (3.2 - 10)$$

Letting

$$\omega = 2\pi \left(\frac{RPM}{60}\right)$$

$$r \approx \frac{r_2 + r_1}{2}$$

and $$\left(\frac{D}{\nu}\right)^{1/3} \approx \left(\frac{10^{-5}}{10^{-2}}\right)^{1/3} = 10^{-1}$$

gives

$$\frac{y_d}{\delta} \geq 2.42 \left(\frac{r_2 - r_1}{r_2 + r_1}\right) \qquad (3.2 - 11)$$

which for the dimensions in Fig. 10 gives

$$\frac{y_d}{\delta} \geq 0.22$$

The ratio y_d/δ turns out to be a constant, independent of RPM.

3.3 Reexamination of Electrochemical Kinetic Data for Titanium in HCl

The finding with the rotating disk and ring disk experiments that a considerable fraction of the initial anodic current to newly generated titanium surfaces goes to soluble Ti^{+3} required reexamination of the previously obtained kinetic data for Ti:8-1-1 in 12 M HCl (4). Reexamination of the data also revealed further "fine structure" that was glossed over in the original analysis. The purpose of the original analysis was to obtain approximate kinetic data on formation of TiO_2 and hydrogen ion reduction suitable for use in the preliminary evaluations of the MTK model. Results of the more recent analysis of the kinetic data will be presented here. Much of it is somewhat speculative but will serve as a basis for design of further critical kinetics experiments.

In the previous presentation (4) reproductions of oscilloscope current versus time traces at potentials of -800 mv and -960 mv (SCE) were shown, In the trace at -960 mv in which the initial current was cathodic, the cathodic current was shown to reach the maximum at approximately one millisecond as compared to a much shorter time required to reach peak cathodic current at more negative potentials or to reach peak anodic current at potentials more positive than -800 mv. While an analysis of the slow cathodic rise time was not made earlier it appears appropriate to do so now.

Two explanations of the slow rise time are the hydrogen ion discharge is slow to get started, or that there is an initial anodic current which dies out. The measured current is, of course, the difference between the actual anodic and cathodic currents.

$$i = i_a - i_c \qquad (3.3\text{-}1)$$

The second explanation is believed to be the case because at potentials somewhat more positive than -925 mv, there is an initial anodic peak followed by a cathodic peak. It is also difficult to explain a delay time for hydrogen ion discharge in a concentrated acid solution.

An oscilloscope trace for a potential of -900 mv showing the anodic and cathodic peaks is shown in Fig. 16a. The scale is expanded in Fig. 16b to show the proposed resolution of anodic and cathodic currents. It is assumed that after the cathodic peak the actual anodic component is a small fraction of the cathodic component (the decrease in cathodic current is assumed as before (4) to be due to oxide coverage at a low current density). The initial slope of the cathodic current after its peak is extrapolated back to zero time. The difference between measured current before the cathodic peak and this extrapolated line is considered to be the initial anodic current. It can only be measured over a narrow range of potentials, more negative than the mixed potential (~-800 mv) but more positive than the potential at which the initial anodic peak dissappears (~-925 mv).

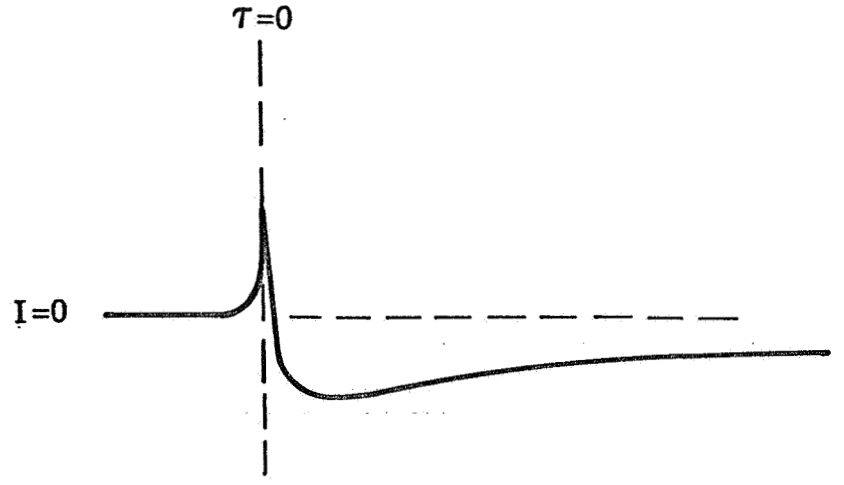

a) Oscilloscope Trace
Horizontal 2 ms/cm
Vertical 0.05 v/cm across 10 0hms

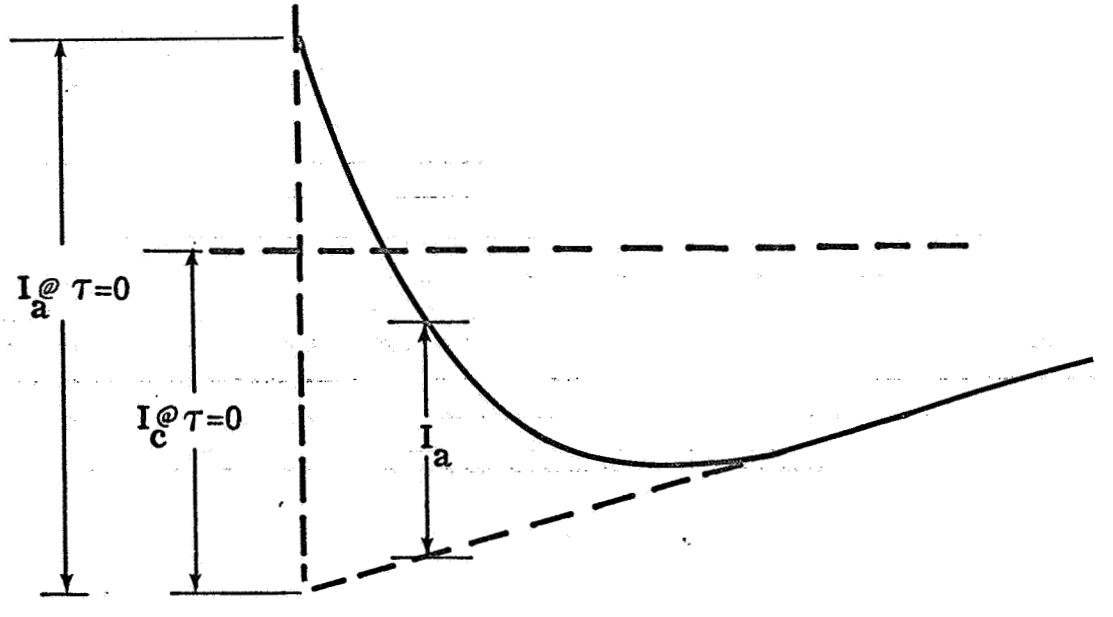

b) Definition of I_c@τ=0 and I_a on Expanded Scale

Fig. 16 Data for fracture of Ti:8-1-1 in 12 M HCl at -900 mv (SCE)

It is proposed that analogous to the interpretation by Hagyard and Earl (20) of their initial potentials of freshly generated aluminum surfaces, that the initial anodic current observed in the potential range of -925 to -800 mv is formation of the metal ion, in this case Ti^{+3}. It is proposed further that the decay in the initial anodic current is due to inhibition by hdride formation, based on the observed relation of decrease in initial anodic current to potential. The time for the initial anodic current I_a to drop to 10% of the value at time zero is plotted in Fig. 17. It is noted that the time increases with increase in potential in the positive direction. This relation would be expected with a cathodic process causing inhibition, rather than with an anodic process. With this criterion, time to form a monolayer of hydride based on the initial cathodic current at time zero was also plotted in Fig. 17.

$$\tau_M = \frac{Q_H A}{I_c(\tau=0)} \qquad (3.3 - 2)$$

where τ_M = time to form a monolayer of TiH_2; Q_H = charge density of a monolayer of TiH_2 (assumed to be $\sim 4 \times 10^{-4}$ coul/cm^2 for two H per basal Ti atom); A = area of new surface ($\sim$0.05 cm^2); and $I_c(\tau=0)$ = extrapolated initial cathodic current (Fig. 16). Both curves on Fig. 17 have approximately the same slope (160 mv/decade for $I_a/I_a(\tau=0) = 0.1$ and 180 mv/decade for τ_M), although they are separated by a factor of

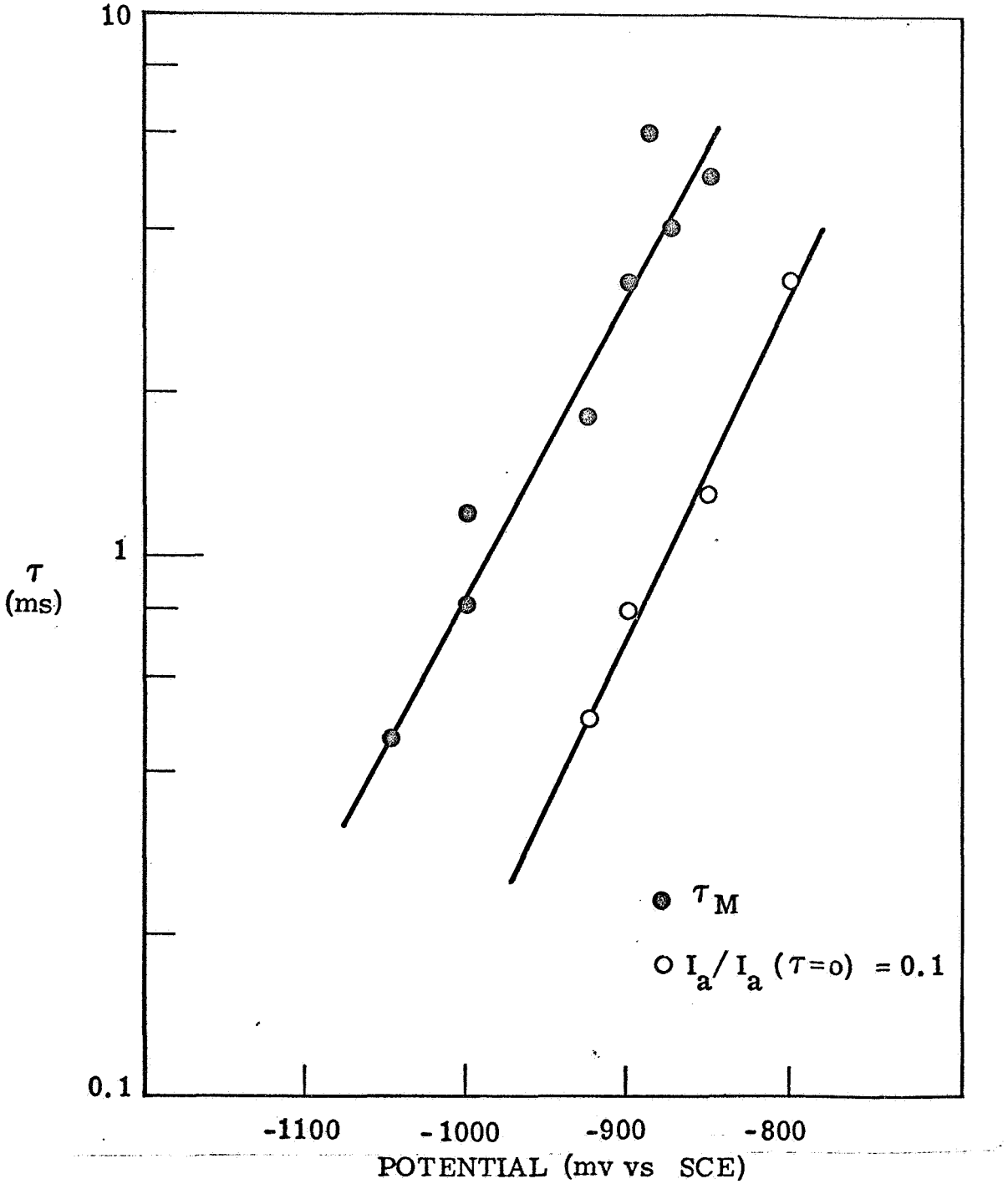

Fig. 17 Plot of log τ_M and log $(I_a/I_a(\tau=0) = 0.1)$ vs applied potential

about five. A possible explanation for this separation is that the initial anodic and cathodic currents are both considerably larger than indicated in Fig. 16 and both inhibited by formation of hydride.

The initial anodic current peaks for those experiments at potentials between -925 and -800 mv are plotted in Fig. 18. A Tafel line with a 120 mv slope drawn through the points has an intercept at the reversible potential for Ti/Ti^{+3} (-1450 mv SCE) at about 10^{-5} amp/cm^2. This exchange current density for metal dissolution would appear to be rather low (compared to an expected > 10^{-3} for metal dissolution) but the initial anodic currents may be low as noted above and it is a long extrapolation and the reversible potential is not too precisely known. A dashed Tafel line for hydrogen ion discharge with a 120 mv slope is drawn to be consistent with the observation of a net initial anodic current at about -925 mv.

More "fine structure" was found in the cathodic current curves over longer time periods as shown in Fig. 19. There appear to be three distinct regions with different behavior of current with time. In region I the current decreases with time with decreasing slope. This was the region for which the initial slope was extrapolated to the zero current intercept to get an estimate of current for rate of

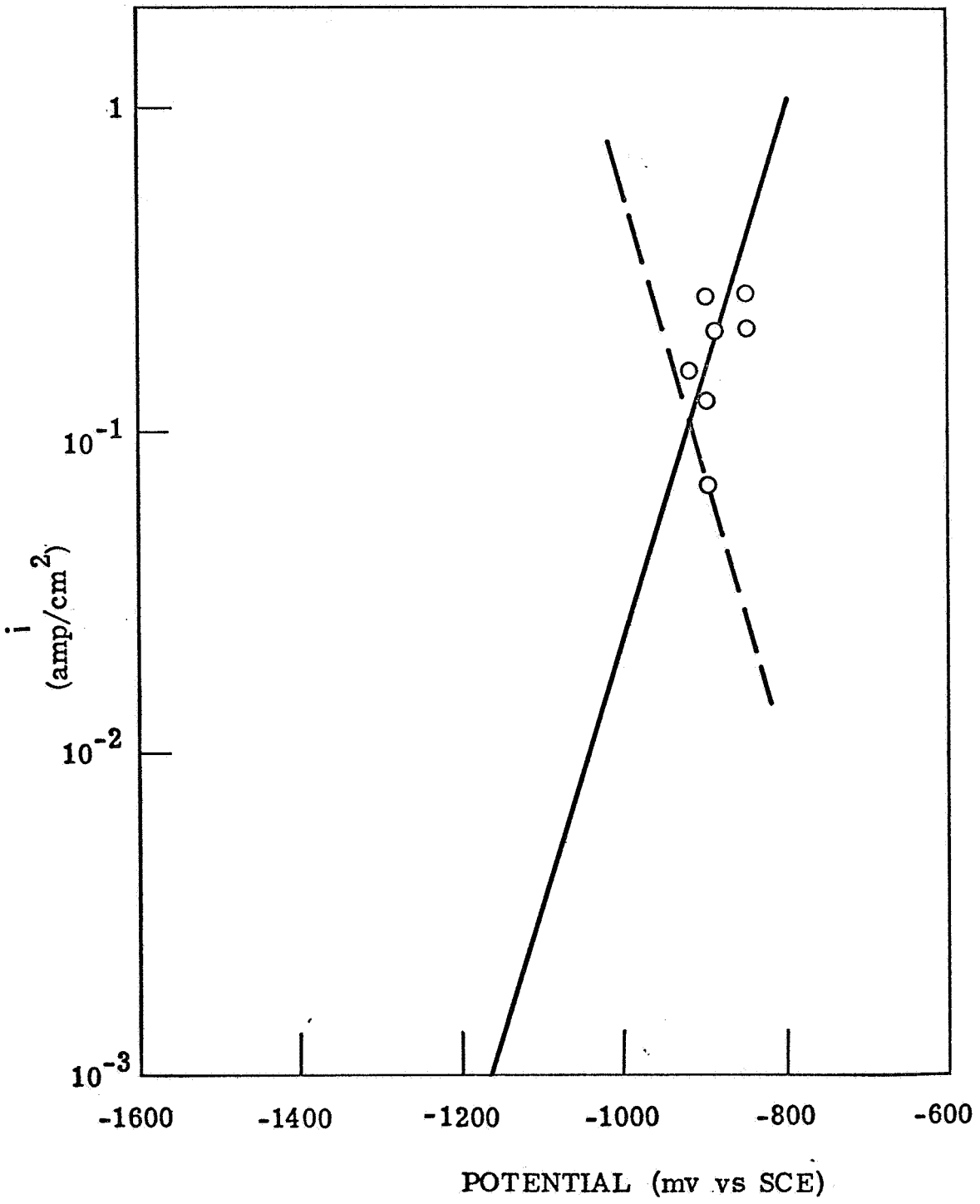

Fig. 18 Tafel Plot of initial anodic current density

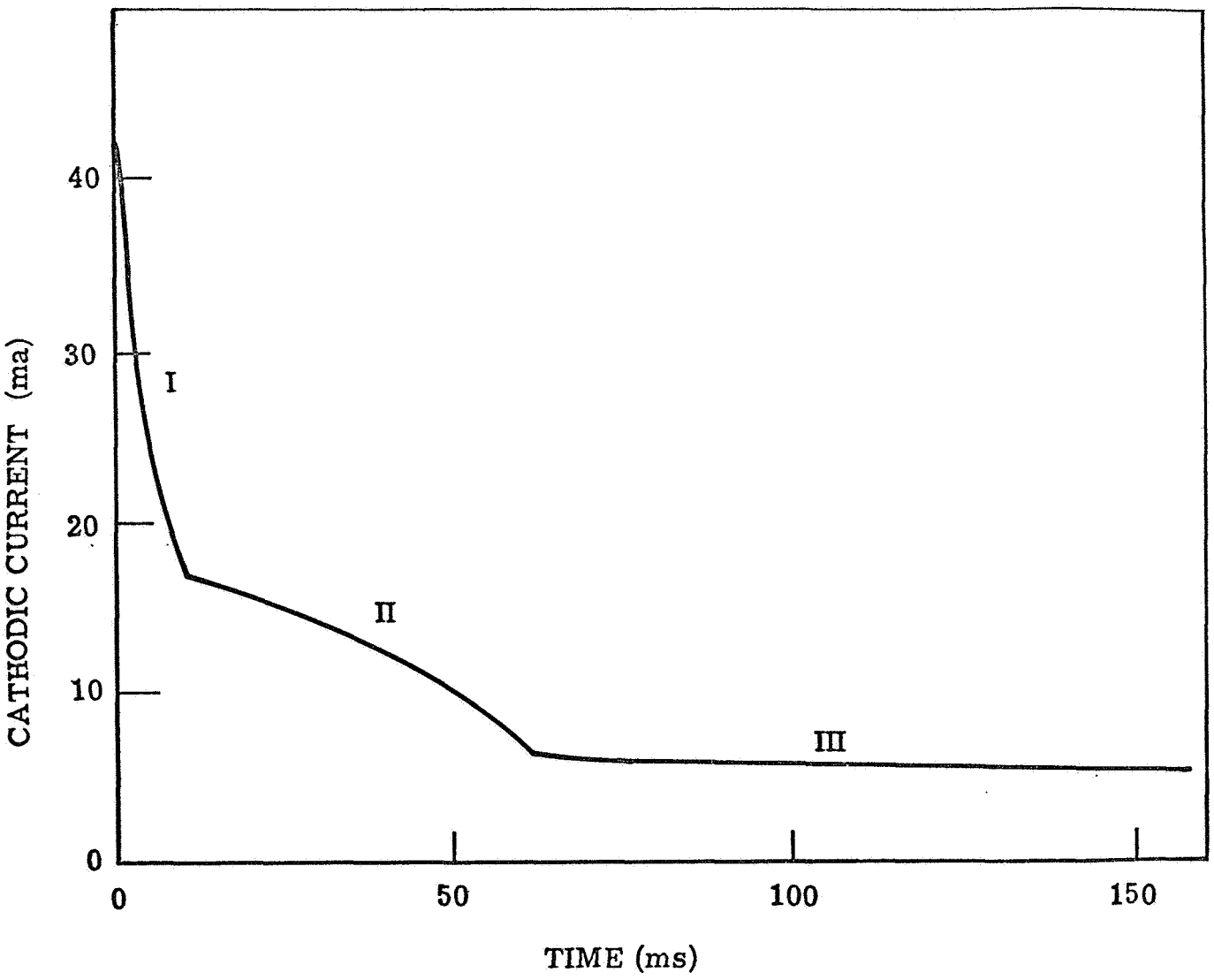

Fig. 19 Replot of oscilloscope curves of cathodic current after fracture of Ti:8-1-1 in 12M HCl at -1050 mv (SCE)

initial oxide formation previously (4). Region II has not been discussed previously and is characterized by abrupt changes in slope at each end and a generally slowly increasing slope in between. Region III is an approximately steady state current region and is the current considered previously (4) to be the discharge of hydrogen ion on oxide covered surface.

Cathodic currents for potentials of -1050 to -850 are replotted on semilog paper in Fig. 20. The three regions are again clearly seen. The transition time from regions I to II appears to be independent of potential in the range available. The data for region I appear to be linear on the semilog plot but there are not enough data to be definitive. The region II data are all curved with increasing slope. The transition time from regions II to III apparently decreases with increasing potential as can be seen in Fig. 21.

The region II data were replotted in Fig. 22 as logarithm of cathodic current versus τ^2 measured from fracture. This appeared to straighten the region II data, although there still appeared to be a dip at the end to region III.

A straight line relation would be expected in Fig. 22 for patch growth of oxide which inhibits H^+ ion discharge. Combining

$$i_H = i_{H1} (1-\theta) \qquad (3.3 - 3)$$

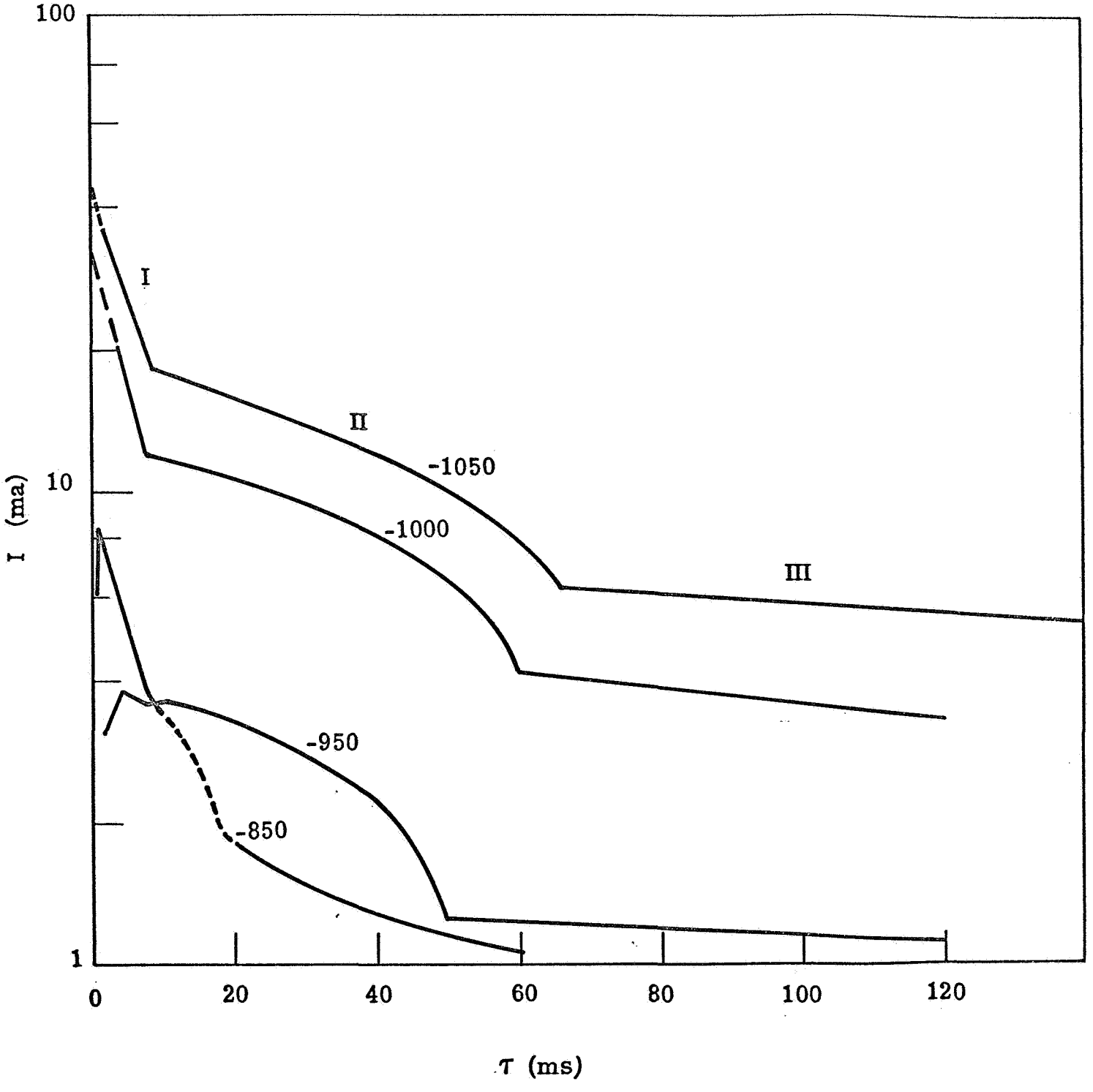

Fig. 20 Decay of cathodic current for Ti:8-1-1 in 12M HCl ($A = 0.05cm^2$) at potentials of -1050 to -850 mv (SCE)

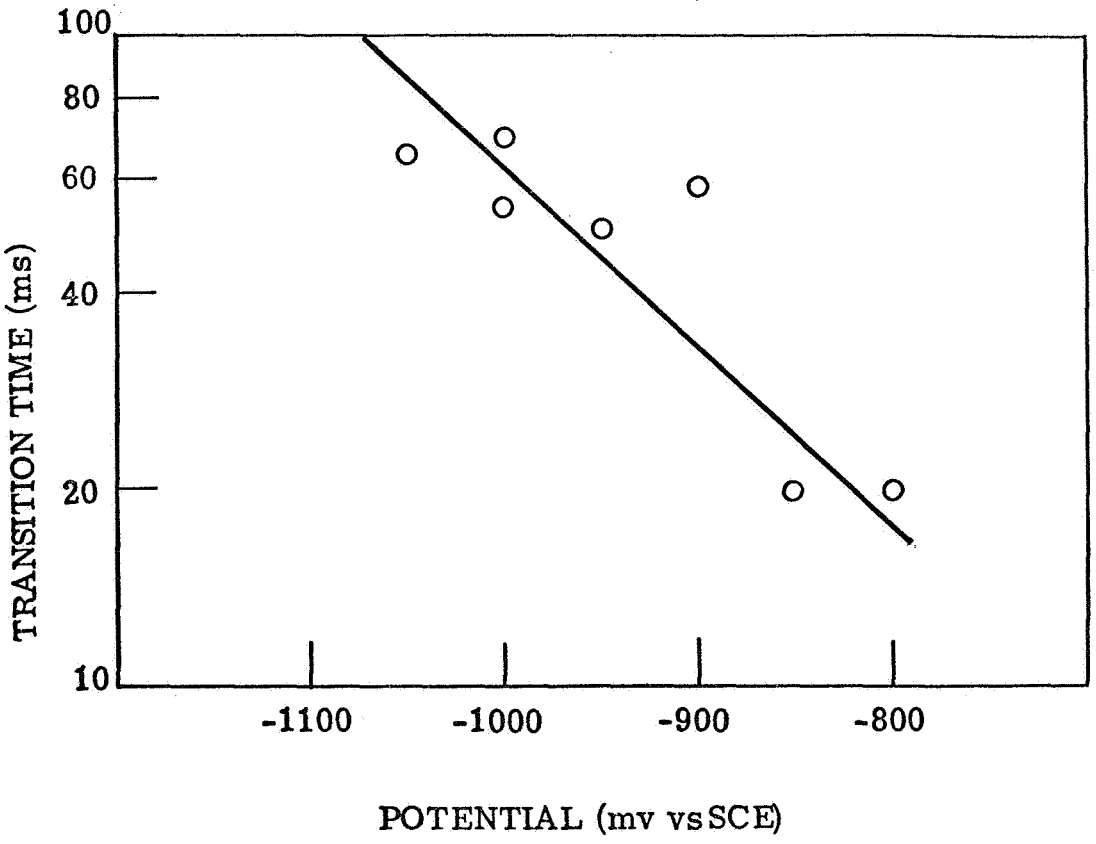

Fig. 21 · Transition time from regions II to III

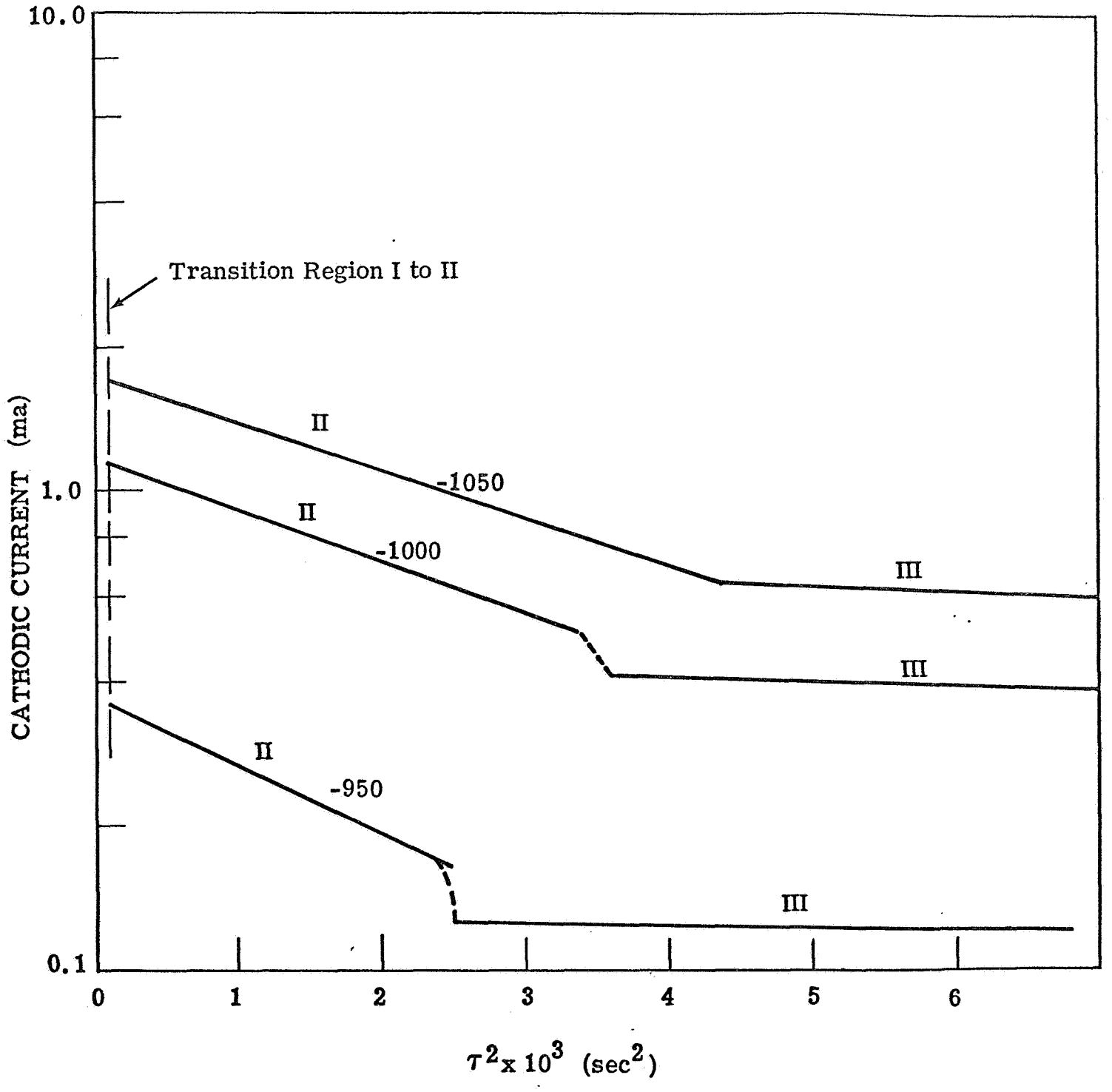

Fig. 22 Replot of region II data from Fig. 20 vs τ^2

(where $i_{H1} = i_{H0}\exp\left[\frac{\alpha n F \eta}{RT}\right]$) with equation 3.1 - 5 gives

$$i_H = i_{H1}\exp\left[-n\pi\left(\frac{i_2\delta_m}{Q_o}\right)^2\tau^2\right] \qquad (3.3 - 4)$$

Taking logarithms and differentiating gives

$$\frac{d(\log i_H)}{d(\tau^2)} = -\frac{n\pi}{2.30}\left(\frac{i_2\delta_m}{Q_o}\right)^2 \qquad (3.3 - 5)$$

The slope of the region II line at -1000 mv in Fig. 22 gives

$$\frac{d(\log i_H)}{d(\tau^2)} \approx 10^2 \text{ sec}^{-2}.$$

Use of values of n and i described by Vermilyea (15) for growth of $PbSO_4$ patches on lead in 2N H_2SO_4 gives a value of the slope from equation that is too small, e.g., for $n = 10^{-9}$ cm^2 and $i = 4 \times 10^{-3}$ amp/cm^2 (values for $PbSO_4$) and $\delta_m \approx 5 \times 10^{-8}$ cm and $Q_o \approx 4 \times 10^{-4}$ coul/cm^2 (approximate values for TiO_2), gives

$$\frac{d(\log i_H)}{d(\tau^2)} = -3.4 \times 10^{-4} \text{ sec}^{-2}.$$

This calculated slope is nearly six orders of magnitude too small. The values of δ_m and Q_o are the right order of magnitude so it is the values of n or i_2 that must be adjusted to fit the experimental

data. The value of n must be $<<10^{15}$ cm^{-2} in order to have discreet patches of oxide; therefore i_2 for TiO_2 must be greater than 4×10^{-2} amp/cm^2 (for $PbSO_4$).

An estimate of i_2 for TiO_2 is made as follows. The value of i_2 is related to the average current density by

$$i_2 = \frac{i}{2\pi nrh} \qquad (3.3 - 6)$$

where r = radius of patches and h = height. But n and r are related at the time of impingement of the patches. Consider impingement of a square array of patches for which

$$n\,(2r)^2 = 1 \qquad (3.3 - 7)$$

combining equations 3.3 - 6 and 3.3 - 7 gives

$$i_2 \approx \frac{i}{\pi h\, n^{\frac{1}{2}}} \qquad (3.3 - 8)$$

For $i \approx 10^{-1}$ amp/cm^2 at -1000 mv (Fig. 10, Ref. 4), $h = 5 \times 10^{-8}$ cm (a monolayer for passivation of titanium) and $n = 10^9$ cm^{-2} gives $i_2 \approx 20$ amp/cm^2. This value in equation 3.3 - 5 gives the right order of magnitude for $\frac{d(\log i_H)}{d(\tau^2)}$ as compared to the value of the slope in Fig. 22. While by no means proving the mechanisms of patch growth of TiO_2 as inhibiting hydrogen ion discharge the numbers do not appear unreasonable.

The analysis of the current on the anodic side of the mixed potential is also speculative. The behavior of the anodic current with time will be analyzed from the viewpoint of the random growth oxide monolayer and the patch growth models. The patch growth model appears at this time to fit the data with fewer inconsistencies.

The analysis of the data involves many difficulties:

1. Much of the work to date has been done with Ti:8-1-1 because this is the alloy that was used for a large fraction of the SCC experiments. This may have produced some side effects due to a nonhomogeneous surface.
2. The current densities on the new surfaces were very large, resulting in appreciable IR drop in the electrolyte which must be accounted for in the analysis.
3. Several different simultaneous reactions are possible.
4. The geometry of the system was apparently not perfectly reproducible from run to run leading to some scatter in the data.

Fortunately much of the significant transient behavior occurs at time periods of greater than 10^{-4} seconds, allowing use of an ordinary electronic potentiostat.

First we will consider the analysis by the random oxide growth model. A semilog plot of anodic current versus time is given in Fig. 23 for Ti:8-1-1 specimens in 12 M HCl. It can be seen that anodic current increases with more positive potentials but the rate of decrease in current falls off at more positive potentials. An

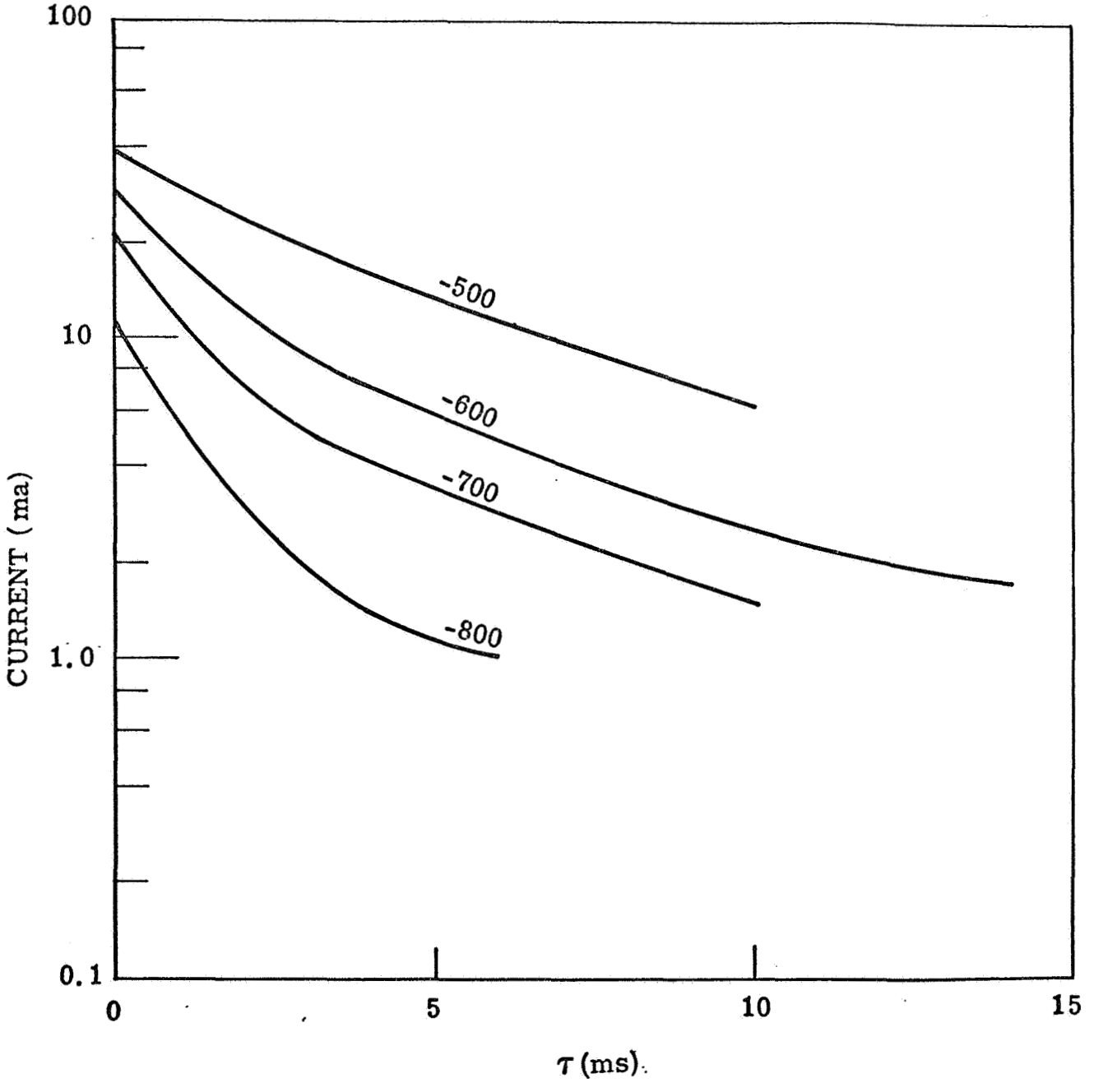

Fig. 23 Anodic current for Ti:8-1-1 in 12M HCl (A = 0.05 cm)

equation is derived in Appendix I for estimating the initial current density for formation of oxide using the random growth model

$$i_{ox1} = - \left(\frac{1+\bar{R}Ai_{a1}}{i_{a1}} \right) Q_o \left(\frac{di_a}{d\tau} \right)_{\tau = 0} \qquad (3.3 - 9)$$

where $\bar{R}$ is the effective resistance of the electrolyte estimated from the slope of the peak current density versus applied potential, A is the Tafel parameter $\left(\frac{\alpha nF}{RT}\right)$, i_{a1} is the peak initial anodic current density, Q_o is the charge density of a monolayer of oxide, and $\left(\frac{di_a}{d\tau}\right)_{\tau = 0}$ is the initial slope of the current density time plot.

The initial anodic current density and the calculated value of the initial passivating current density from equation 3.3-9 for Ti:8-1-1 in 12 M HCl are plotted in Fig. 24. It is seen that the calculated passivation current density is greater than the actual current density. One solution to this problem is to assume that the surface has areas to two different reactivities, the more reactive surface passivating first. Such a situation might result from the different aluminum composition between grains in Ti:8-1-1 (21). One would therefore multiply the calculated i_{ox1} by the fraction of the surface covered by the active grains to get the average current density if it were distributed uniformly over the whole surface. Assuming a fraction 0.2 active surface brings all of the calculated initial current densities for passivation below the total initial anodic current density. Areas of two different activity might explain the region I and region II passivation discussed earlier.

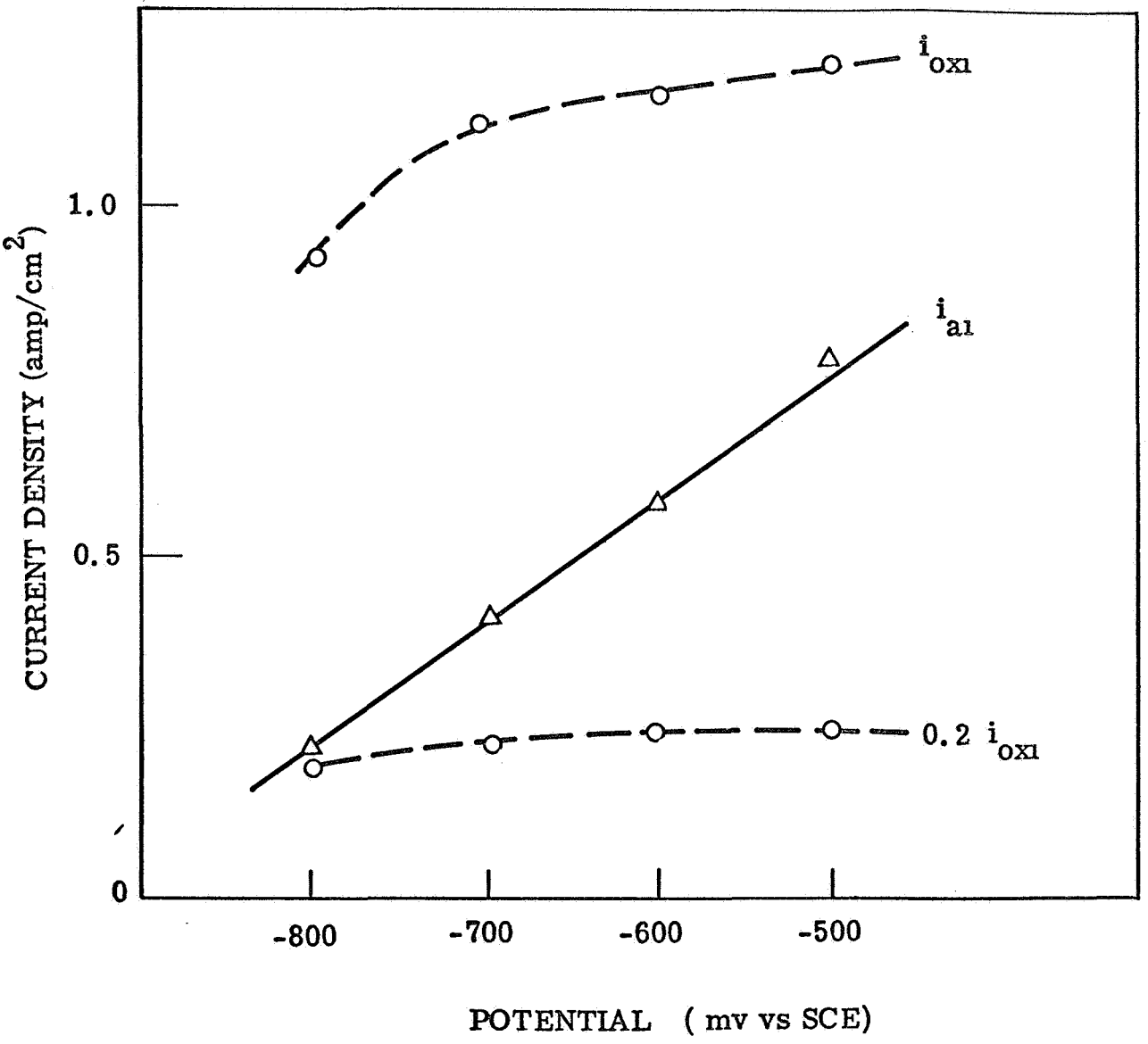

Fig. 24 Comparison of calculated initial current density for passivation to total initial anodic current density for Ti:8-1-1 in 12M HCl

Similar experiments and calculations conducted with commercially pure titanium specimens of the same configuration in 3M HCl gave the data shown in Fig. 25. Here the calculated initial passivating current density turned out to be approximately equal to the total initial anodic current density over the range of potentials studied. This is consistent with an expected more homogeneous surface. That such a large proportion of the initial current density apparently goes to the passivation reaction is inconsistent with the scraped rotating disk experiments which showed that a large fraction of the current density went to soluble Ti^{+3}. The latter is a time averaged result for the surface so this would require that the current density is weighted more heavily in favor of soluble Ti^{+3} after the initial peak current which does not appear reasonable.

The most serious inconsistency with this model is that if most of the initial current density goes to form a monolayer of oxide the surface will become covered in too short a period of time. If for example the initial current density is 3 amp/cm^2 (such as for Ti at a potential of 0 mv) the time for complete coverage would be

$$\tau = \frac{Q_o}{i} = \frac{4 \times 10^{-4}}{3} \approx 10^{-4} \text{ sec},$$

whereas the current did not start to decrease until about 5×10^{-4} sec for this run (Fig. 26).

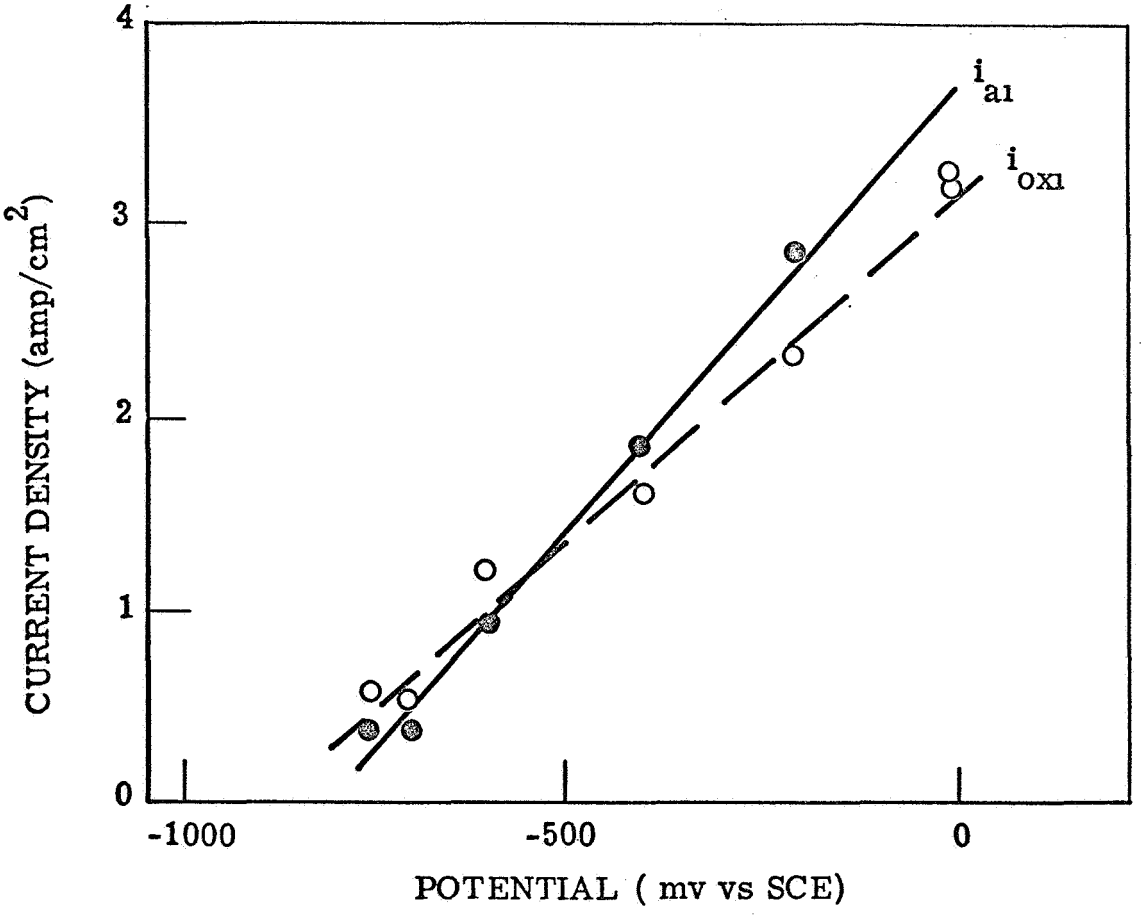

Fig. 25 Comparison of calculated initial current density for passivation to total initial anodic current density for Ti in 3M HCl

It has been pointed out earlier (22) that the resistance calculated from the plot of peak initial current density versus potential is larger than the value calculated for hemispherical conduction in the electrolyte to the two new surfaces. A part of the difference can be explained by the close proximity of the two broken faces and the restriction on the electrolyte area. The resistance on the anodic side was unexplainably 2½ times larger for the Ti:8-1-1, however. In the recent runs with commercially pure titanium in 3 M HCl the resistance on the anodic side was almost identical to the Ti:8-1-1 data on the cathodic side. Calculations shown in Appendix III indicate, however, that the difference cannot be explained by increased current density to more active areas. The conductivities of 12M and 3M HCl are nearly the same so it is apparently not due to differences in electrolyte resistance.

An equation is derived in Appendix II for patch oxide growth. Using the simplifying assumptions that most of the initial current goes to form soluble Ti^{+3}, and therefore the oxide current can be neglected, and that all the terms but τ in the exponent of equation are constant gives

$$\tau = C^{-\frac{1}{2}} \left[A_+(E_A - E_+^e) - A_+ \bar{R}\, i_a - 2.3 \log (i_a/i_{+0})\right]^{\frac{1}{2}} \quad (3.3 - 10)$$

where $C = n\,\pi(i_2\delta_m/Q_o)^2$, the only adjustable parameter. Values of $\bar{R}$ and i_{+o} can be determined from data on peak current density, i_{a_1}, at $\tau = 0$. The following values were used for a series of experiments with commercially pure titanium conducted in 3M HCl:

$A_+ = 19.5$ volts^{-1}

$\bar{R} = 0.24$ volts/(amp/cm^2) (calculated from data at $\tau = 0$)

$E_+^e = -1.4$ volts (SCE)

$i_{+0} = 4 \times 10^{-5}$ amp/cm^2 (calculated from data at $\tau = 0$)

The value of i_{+0} appears somewhat low for metal dissolution as noted earlier on the cathodic side.

Experimental data for pure titanium fractured in 3M HCl at a potential of 0 mv (SCE) are compared to equation 3.3 - 10 (using a value of $C^{-\frac{1}{2}} = 0.5 \times 10^{-3}$) in Fig. 26. The equation fits over a

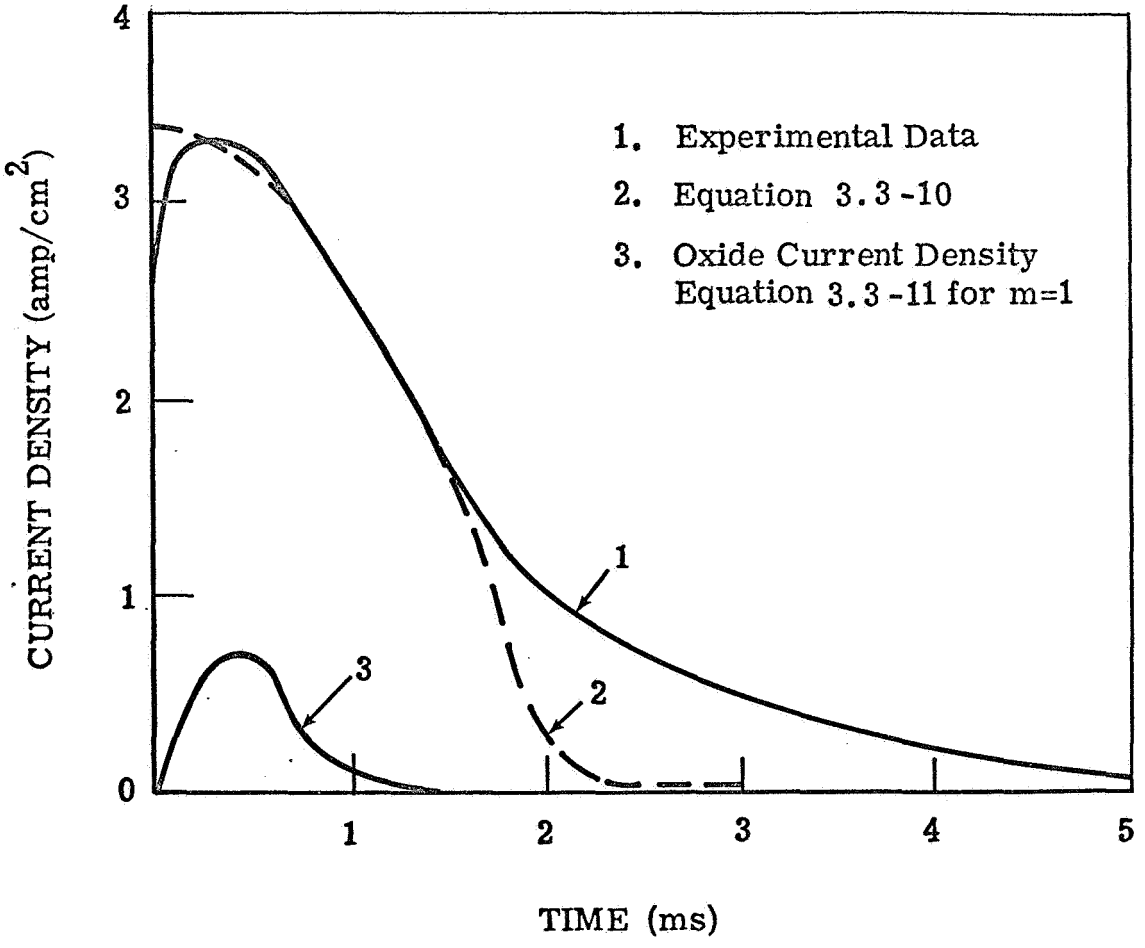

Fig. 26 Comparison of equation 3.3 - 10 with experimental data for fracture of titanium in 3M HCl at a potential of zero mv (SCE)

portion in the middle of the experimental data and the misfit at short and long time might be attributed to the simplifying assumptions.

At short times the current for formation of oxide cannot be negligible. For example, equation 3.1 - 6 rewritten,

$$i_{ox} = 2mQ_o C\tau \exp[-C\tau^2] \qquad (3.3 - 11)$$

is plotted in Fig. 26 assuming $m = 1$, $Q_o = 4 \times 10^{-4}$ coul/cm^2 and $C = 4 \times 10^6$ (from $C^{-\frac{1}{2}} = 0.5 \times 10^{-3}$ above). This oxide current density is not negligible, even for monolayer patches. Further, because even monolayer patches consume a considerable fraction of the current, the patches cannot be many monolayers in thickness. It may be noted that a finite time was required to reach the peak current in this experiment, which may be related to the rise to the peak oxide current. This rise time was obscurred in most of the runs because of noise at less than half a millisecond.

The lack of fit of the equation at about 2 milliseconds from the break might be attributed to undermining the edges of the patches by the high current density corrosion between them as θ approaches unity or to the onset of oxide film thickening through the high field conduction mechanism.

From the value of C we can make an estimate of the peripheral patch current density.

$$i_2 = \left(\frac{C}{n\pi}\right)^{\frac{1}{2}} \frac{Q_o}{\delta_m} \qquad (3.3 - 12)$$

For $C = 4 \times 10^{6}$, $n = 10^{9}$ cm^{-2} (as earlier), $Q_o = 4 \times 10^{-4}$ $coul/cm^2$ and $\delta_m = 5 \times 10^{-8}$, cm,

$$i_2 \quad 300 \text{ amp/cm}^2$$

This is an order of magnitude larger than the value calculated at -1000 mv earlier but $i_2 \approx$ might be expected to increase with anodic potential.

Although we have considered only three reactions - hydrogen ion reduction (including formation of hydride), formation of Ti^{+3} and formation of TiO_2 - the analysis has not been simple and unambiguous. In summary, the present analysis of the kinetic data for relatively concentrated acid solutions suggests the following:

1. Hydrogen ion reduction dominates as the initial reaction at potentials more negative than -925 mv (SCE).
2. The hydrogen ion reduction is partially suppressed by formation of an oxide film.
3. Formation of Ti^{+3} appears to be the dominant initial reaction at potentials more positive than -925 mv (SCE).
4. At potentials between -925 and -800 mv the initial formation of Ti^{+3} is apparently suppressed by formation of a hydride layer.
5. At potentials more positive than -800 mv the initial formation of Ti^{+3} is apparently suppressed by formation of an oxide layer.
6. Equations for patch growth of oxide appear to fit the kinetic data with fewer contradictions than the equations for random monolayer growth.

It is intended to conduct further quantitative tests of the relationships explored in this report by conducting kinetic experiments in a wider range of concentrations, pH and potential.

4.0 CONCLUSIONS

The following conclusions are based on the work accomplished in the period of July 1 through September 30, 1968:

1. It was found in rotating disk and ring-disk experiments in which a titanium disk was scraped with a sapphire cutter in 6 M HCl solution that a large fraction of the current flowing to the surface can be accounted for by formation of Ti^{+3} ions.

2. Reexamination of the previously obtained kinetic data for newly generated surfaces of Ti:8-1-1 in 12 M HCl and examination of new data for commercially pure titanium in 3M HCl indicated that these data can be interpreted in a way consistent with 1.

3. Growth of the passivating oxide film can be described by a patch growth mechanism which will be tested in further experiments.

4. The equations for the patch growth mechanism with simultaneous formation of Ti^{+3} appear to be of a form that can readily be put into the electrochemical MTK model for stress corrosion crack propagation.

5.0 FUTURE WORK

The following items of work are planned for the immediate future:

1. Investigate susceptibility of the Ti:8Mn alloy over a wider range of temperatures in the $\alpha+\beta$ phase field.
2. Investigate the influence of β-grain size on susceptibility.
3. Evaluate the stress criterion for fracture - on notched and un-notched specimens.
4. Investigate the influence of hydrogen charging on SCC.
5. Establish the fracture plane for SCC in Ti:8Mn alloy.
6. Resolve the problem of chloride analysis of titanium.
7. Extend electrochemical kinetic studies to a wider range of halide concentrations and potentials and to other alloys.
8. Include parallel soluble titanium ion formation in mass-transport-kinetic model.
9. Focus attention conceptually and experimentally on events at the crack tip.

6.0 REFERENCES

1. Beck, T.R., Boeing Document D1-82-0554, July 1966.
2. Beck, T.R., and Blackburn, M.J., Research Proposal D1-82-0467, August 1965.
3. Beck, T.R., Contract NAS7-489 Quarterly Progress Report No. 1, September 1966.
4. Ibid, No. 2, January 1967.
5. Ibid, No. 3, April 1967.
6. Ibid, No. 4, July 1967.
7. Ibid, No. 5, October 1967.
8. Ibid, No. 6, January 1968.
9. Ibid, No. 7, April 1968.
10. Ibid, No. 8, July 1968.
11. Pourbaix, M., "Atlas of Electrochemical Equilibria," Pergamon Press, New York (1966).
12. Pourbaix, M., presentation at CITCE Meeting, Istanbul, September 1967.
13. Oliver, J.W., and Ross, J.W., J. Am. Chem. Soc., 85, 2565, (1963).
14. Latimer, W.M., "Oxidation Potentials," 2nd Ed., Prentice Hall, Englewood Cliffs, N.J., (1952).
15. Vermilyea, D.A., "Anodic Films," in "Advances in Electrochemistry and Electrochemical Engineering," 3, Delahay, P. and Tobias, C.W., Ed., John Wiley, New York (1963).
16. Kolthoff, I.M. and Elving, P.J., "Treatise on Analytical Chemistry," Part II, Vol. 5, pp 51-52, Interscience, New York (1961).

17. Lingane, J.J. and Kennedy, J.H., Analytica Chimica Acta, 15, 294, (1956).

18. Albery, W.J. and Bruckenstein, S., Trans. Faraday Soc., 62, 1920, (1960).

19. Levich, V.G., "Physicochemical Hydrodynamics," Prentice Hall, Englewood Cliffs, N.J. (1962).

20. Hagyard, T. and Earl, W.B., J. Electrochem. Soc. 114, 694 (1967).

21. Personal communication, Blackburn, M.J.

22. Beck, T.R., J. Electrochem. Soc., 115, 890 (1968).

APPENDIX I

Derivation of Equation for Initial Passivating Current - with Random Monolayer Oxide Growth

In the electrochemical kinetics experiments the initial current is limited by IR drop in the solution (specimen to Luggin capillary) for potentials slightly removed from the mixed potential because of the unavoidably high current densities on freshly generated surfaces. It is desirable to be able to separate on the anodic side the partial currents for oxide formation and for formation of Ti^{+3}. An equation is derived here for calculating the initial current for oxide formation from experimentally measured parameters.

The total anodic current density is assumed to be the sum of the current for oxide formation and the current for Ti^{+3}

$$i_a = i_{ox} + 1_+ \qquad (I - 1)$$

Each reaction is assumed to occur initially only on the bare surface so that

$$i_{ox} = i_{oxo}\,(1-\theta)\,\exp\,[A_{ox}\,(E - E^e_{ox})] \qquad (I - 2)$$

and

$$i_+ = i_{+0}(1-\theta)\,\exp\,[A_+\,(E - E^e_+)] \qquad (I - 3)$$

where i_o is the exchange current density, θ is the coverage, $A = \frac{\alpha n F}{RT}$, E is the potential at the electrode surface and E^e is

the equilibrium potential for the reaction. The potential at the electrode surface is assumed to be

$$E = E_A - i_a\bar{R} \tag{I-4}$$

where E_A is the potential applied by the potentiostate and $\bar{R}$ is an effective electrolyte resistance between specimen and the Luggin capillary, determined by electrolyte resistivity and the geometry of the system. The value of $\bar{R}$ can be determined approximately from the slope of the potential, E_A, versus peak initial current density for potentials far removed from the mixed potential. The effect of nonuniform current distribution across the newly generated surface will, of necessity, be neglected.

The coverage will be defined by

$$d\theta = \frac{i_{ox}\ d\tau}{Q_o} \tag{I-5}$$

Where Q_o is the charge density of a monolayer of oxide. The initial condition is that $\theta = 0$ at $\tau = 0$.

Equation I-4 may be substituted into Equations I-2 and I-3 and the resulting equations differentiated in respect to the i and θ terms. The di_{ox} and di_+ terms can be eliminated by $di_a = di_{ox} + di_+$, the θ term can be eliminated by the initial condition, the $d\theta$ terms can be eliminated by substitution of Equation I-5, and the exponential terms eliminated by $i_1 = i_o \exp [A(E_A - E^e - i_{a1}\bar{R})]$ where the subscript 1, denotes the initial current giving

$$\left(\frac{di_a}{d\tau}\right)_{\tau=0} = - \frac{\left(\frac{i_{ox1}}{Q_o}\right)(i_{ox1} + i_{+1})}{1 + \bar{R}(A_{ox} i_{ox1} + A_{+} i_{+1})} \qquad \text{(I-6)}$$

Making the assumption that $A_{ox} = A_{+} = A$ and rearranging gives

$$i_{ox1} = - \left(\frac{1 + \bar{R}A\, i_{a1}}{i_{a1}}\right) Q_o \left(\frac{di_a}{d\tau}\right)_{\tau=0} \qquad \text{(I-7)}$$

which is the desired relationship. All quantities on the right can be determined from measurements or estimated, i.e., $\bar{R}$, i_{a1} and $\left(\frac{di_a}{d\tau}\right)_{\tau=0}$ are experimentally determined and $A = 19.5$ volts^{-1} for $\alpha = 0.5$ and $n = 1$ at 25°C, and $Q_o = 4 \times 10^{-4}$ coul/cm^2 for a monolayer of oxide on the basal plane of α-titanium.

APPENDIX II

Derivation of Equation for Anodic Current for Patch Growth of Oxide

The failure of the random monolayer oxide growth model developed in Appendix I to fit the anodic kinetics data in a consistent way prompted an investigation of the patch growth model. Two simplifying assumptions were made in order to make the treatment manageable. It is assumed that throughout the period of growth of the passivating layer that most of the current goes to form soluble Ti^{+3}, i.e.,

$$i_+ > i_{ox}$$

and

$$i_a \approx i_+ \qquad \text{(II - 1)}$$

The second assumption is that n and i_2 in equation 3.1 - 5 are constant, independent of time or potential, so that

$$\theta = 1 - \exp[-C\tau^2] \qquad \text{(II - 2)}$$

The current density for formation Ti^{+3} is

$$i_+ = i_{+o}\,(1-\theta)\,\exp\,[A_+(E-E_+^e)] \qquad \text{(II - 3)}$$

where

$$E = E_A - i_A \bar{R} \qquad \text{(II - 4)}$$

combining equations II - 1, II - 2, II - 3, and II - 4 gives

$$i_a = i_{+0} \exp\,[-C\tau^2] \exp\,[A_+(E_A - E_+^e - i_a\,\bar{R})] \qquad \text{(II - 5)}$$

This equation may be solved explicitly for τ

$$\tau = C^{-\frac{1}{2}} \left[A_+(E_A - E_+^e) - A_+\bar{R}\, i_a - 2.30 \log \left(\frac{i_a}{i_{+0}}\right)\right]^{\frac{1}{2}} \qquad \text{(II - 6)}$$

Equation II-6 gives a relation between current density and time containing only one adjustable parameter; C. The values of $\bar{R}$ and i_{+o} can be determined from data on the peak current at $\tau = 0$.

APPENDIX III

Electrolyte Potential Drop for Current Flowing to Patches on a Surface

It was noted in the text that initial anodic current to Ti:8-1-1 specimens resulted in an apparent higher ohmic resistance than initial anodic current to commercially pure titanium in acid solutions. It was proposed that the higher ohmic resistance could be due to reaction on patches of surface that comprise a fraction of the surface. An equation is derived here to test the feasibility of this hypothesis.

Consider that the active patches are circular in area and uniformly distributed on the surface in a hexagonal array. The fraction of active area is therefore

$$f = n\pi r^2 \qquad \text{(III - 1)}$$

where n = number of patches/cm^2 and r = mean radius of patches. The distance between centers of patches can be derived from the geometry,

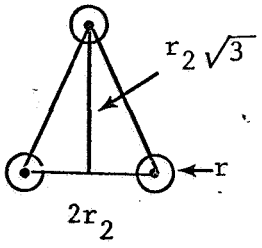

giving

$$f = \frac{3(1/6)\pi r^2}{r_2(\sqrt{3}\, r_2)} = \left(\frac{\pi}{2\sqrt{3}}\right)\frac{r^2}{r_2^2}$$

or

$$r_2 = \left(\frac{\pi}{2\sqrt{3}\, f}\right)^{\frac{1}{2}} r \qquad \text{(III - 3)}$$

Consider now that the patches will be replaced by hemispheres of the same radius

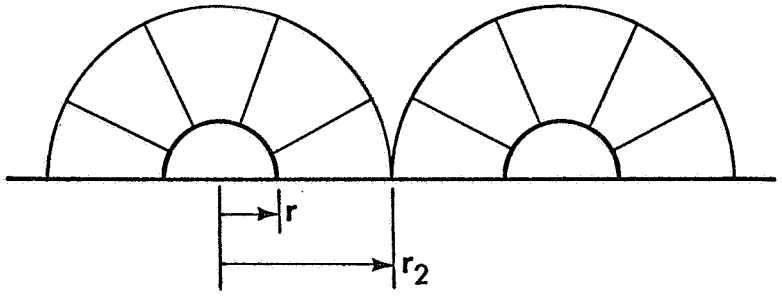

and that hemispherical conduction occurs in the electrolyte between r and r_2 . The resistance of each hemisphere of electrolyte, assuming constant resistivity, ρ, is

$$R = \frac{2\rho}{4\pi}\left(\frac{1}{r} - \frac{1}{r_2}\right) \qquad \text{(III - 4)}$$

The potential drop in a hemisphere is

$$\Delta E = IR = \left(\frac{i}{n}\right)\left[\frac{\rho}{2\pi}\left(\frac{1}{r} - \frac{1}{r_2}\right)\right] \qquad \text{(III - 5)}$$

where I = current to hemisphere and i = mean current density for whole surface. Eliminating r and r_2 by equations III-1 and III-3 gives

$$\Delta E = \frac{1}{2\sqrt{\pi}} i\rho \left(\frac{1}{nf}\right)^{\frac{1}{2}} \left[1 - \left(\frac{2\sqrt{3}}{\pi}\right)^{\frac{1}{2}} f^{\frac{1}{2}}\right]$$

$$= 0.282\ i\rho \left(\frac{1}{nf}\right)^{\frac{1}{2}} \left[1 - 1.05\ f^{\frac{1}{2}}\right] \qquad \text{(III - 6)}$$

or $$\bar{R} = \frac{\Delta E}{i} \approx 0.282\rho \left(\frac{1}{nf}\right)^{\frac{1}{2}} \left[1 - f^{\frac{1}{2}}\right]$$

Assuming: $\rho \approx$ 1.1 ohm cm (12M HCl)

$f =$ 0.2 from analysis of initial current

$n = \left[(1/25) \times 10^{-4}\right]^2$ for 25μ grains in Ti:8-1-1

gives $\bar{R} \approx 10^{-3}$ ohm cm^2 .

This resistance is too small compared to the difference between the resistance observed for Ti:8-1-1 and Ti (R_{dif} = 0.68 - 0.24 = 0.44 ohm cm^2) to explain the difference.